Running Head: Cretaceous mixed-system, Azerbaijan

Title: Evolution of a mixed siliciclastic-carbonate deep-marine system on an unstable margin: the Cretaceous of the Eastern Greater Caucasus, Azerbaijan

Authors: ZOË A. CUMBERPATCH[1*] , EUAN L. SOUTTER[1] , IAN A. KANE[1] and MAX CASSON[1]

Institutions:
[1]Department of Earth and Environmental Sciences, University of Manchester, Oxford Road

Email: zoe.cumberpatch@manchester.ac.uk

Keywords: deep-marine, mixed-system, siliciclastic-carbonate, Caucasus, Azerbaijan,

ABSTRACT

Mixed siliciclastic-carbonate deep-marine systems, herein termed 'mixed systems', are less well documented than their siliciclastic-dominated counterparts, but may be common globally and misinterpreted as transient transition zones between carbonate and siliciclastic deposition. The well-exposed Upper Cretaceous mixed-system of the Buduq Trough, Eastern Greater Caucasus (EGC), Azerbaijan, provides an opportunity to study the interaction between contemporaneous siliciclastic and carbonate deep-marine deposition. The Buduq Trough represents a sub-basin formed within the larger unstable post-rift margin of the EGC. Qualitative and quantitative facies analysis reveals that Upper Cretaceous stratigraphy of the Buduq Trough comprises a Cenomanian-Turonian siliciclastic submarine channel complex, which abruptly transitions into a Coniacian-Maastrichtian mixed-lobe succession. The Cenomanian – Turonian channels are shown to be entrenched in lows on the palaeo-seafloor, with the sequence entirely absent 10 km toward the west, where a Lower Cretaceous submarine landslide complex is suggested to have acted as a topographic barrier to deposition. By the Campanian this topography was largely healed, allowing deposition of the mixed-lobe succession across the Buduq Trough. Evidence for topography remains recorded through opposing palaeocurrents and frequent submarine landslides. The overall sequence is interpreted to represent abrupt Cenomanian-Turonian siliciclastic progradation, followed by ~Coniacian retrogradation, before a more gradual progradation in the Santonian-Maastrichtian. This deep-marine siliciclastic system interfingers with a calcareous system from the Coniacian onwards. These mixed lobe systems are different to siliciclastic-dominated systems in that they contain both siliciclastic and calcareous depositional elements, making classification of distal and proximal difficult using conventional terminology and complicating palaeogeographic interpretations. Modulation and remobilisation also occurs between the two contemporaneous systems, making stacking patterns difficult to decipher. The Buduq Trough is analogous in many ways to offshore The Gambia, NW Africa, and could be a suitable analogue for mixed deep-marine systems globally.

Introduction

Mixed siliciclastic-carbonate systems

Sedimentary successions characterised by contemporaneous deposition of both siliciclastic and carbonate lithologies, herein termed 'mixed-systems', have been identified from the Cambrian (Osleger and Montañez, 1996) to the Quaternary (Dunbar & Dickens, 2003; Tucker, 2003). Mixed systems are formed by a variety of depositional processes (e.g. Mount, 1984; Chiarella et al. 2017) and are consequently recognised in a variety of depositional environments, such as: shoreface (Zonneveld et al. 1997), lagoonal (Mitchell et al. 2001), shelfal (Mount, 1984; Zeller et al. 2015), slope (Gawthorpe, 1986) and(Ditty et al. 1997; Yose & Heller, 1989; Bell et al. 2018; Moscardelli et al. 2019). Mixed-systems deposited in deep-marine (below storm-wave base) are usually formed by material shed from a shallower carbonate-producing shelf that periodically received terrigenous sediment (Fig. 1) (Mount, 1984; Dunbar & Dickens, 2003; Crevello & Schlager, 1980). This material is then re-deposited in deep-marine by a spectrum of sediment gravity flows types, from turbidity currents to submarine landslides (Dorsey & Kidwell, 1999; Miller & Heller, 1994; Tassy et al. 2015; Moscardelli et al. 2019).

Mixed lobes

Sediment-gravity-flows that lose confinement on the slope or basin-floor build lobate depositional bodies, known as lobes, which form important archives of palaeoclimatic and palaeogeographic information (e.g. Hessler & Fildani, 2019). Exhumed deep-marine lobes have been studied in great detail, and a wide variety of stacking patterns, depositional processes and facies distributions have been described and interpreted (e.g. Mutti, 1983; Postma et al. 1993; Prélat et al. 2009; Terlaky et al. 2016; Kane et al. 2017; Bell et al. 2018; Fildani et al. 2018; Fonnesu et al. 2018; Soutter et al. 2019, Cumberpatch et al. in prep.). These studies typically focus on siliciclastic systems, with few studies investigating the characteristics of lobes formed in mixed-systems (Fig. 1). This study aims to address this by describing exhumed Cretaceous submarine lobes from the Eastern Greater Caucasus (EGC), Azerbaijan (Fig. 2) which were built by contemporaneous deposition of calcareous and siliciclastic sediment gravity flows. The characteristics of these mixed lobes and the processes that govern their deposition are then compared with siliciclastic lobes. This study will also describe the sedimentological evolution of the basin throughout the Cretaceous, providing insights into the stratigraphic evolution of a basin characterised by unstable margins.

Geological Setting and Basin Structure

Evolution of the Eastern Greater Caucasus

The Eastern Greater Caucasus forms the easternmost extent of the NW-SE trending Greater Caucasus orogenic belt, which runs from the Black Sea in the west to the Caspian Sea in the east (Fig. 2) (e.g. Bochud 2011). The EGC sits on the southern-edge of the Scythian Platform, which represents the southern margin of the Eastern European continent (Saintot et al. 2006). The exposed EGC is mainly composed of Mesozoic-aged sediments that accumulated during multiple phases of extension and convergence related to sequential closure of the Tethys toward the south (Golonka, 2004; Vincent et al. 2007). Most of these Mesozoic tectonic events occurred in the Jurassic, with Upper Triassic-Lower Jurassic compression followed by Lower- to Mid-Jurassic rifting and compression, and Upper Jurassic rifting and compression (Bochud 2011). These tectonic events are recorded by major thickness variations across the Middle Jurassic interval (Fig. 3).

The Lower Cretaceous of the EGC was deposited within an unstable marine environment, as recorded by frequent mass-wasting events and major thickness changes across the interval (Egan et al. 2009; Bochud 2011). Subsidence increased through the Lower Cretaceous and into the early Upper Cretaceous due to back-arc extension associated with the opening of the West Black Sea Basin to the west (Nikishin et al. 2001), resulting in deep-marine deposition of extensive mudstones interspersed by submarine landslide deposits and terrigenous sediments (e.g. Brunet et al. 2003).

The remainder of the Cretaceous sequence was deposited during a period of thermal subsidence on a southward-dipping slope, with the basin divided into a series of sub-basins (Bochud 2011). One of these sub-basins, the Buduq Trough, encompasses our study area. The Cretaceous stratigraphy is dominated by calcareous and siliciclastic turbidites and conglomerates interbedded with hemipelagic marls and mudstones (e.g. Brunet et al. 2003). A number of intra-Cretaceous unconformities are seen within the basin and are related to periods of compression (Egan et al. 2009) or sea-level fluctuations. The end of the Cretaceous sequence is represented by a Base-Cenozoic unconformity formed during Paleogene compression (Bochud 2011).

Collision of the Arabian and Eurasian plates in the Oligocene (Vincent et al. 2007) deformed the Mesozoic and early Cenozoic succession into a series of exhumed synclines bound by major faults. These faults separate distinct structural zones within the EGC (Fig. 2, Fig. 3) (Bochud 2011).

The Buduq Trough

The Buduq Trough is preserved in the east-west trending Qonaqkend structural zone (Fig. 4) and has been interpreted as an Upper Cretaceous 'paleo-valley' incised into Lower Cretaceous deep-marine sediments and Upper Jurassic limestones following a period of compression (Fig. 2B) (Egen et al. 2009; Bochud 2011). It is likely that this compression was related to far-field tectonism in the eastern Black Sea (Sosson et al. 2015), which overprinted the subsidence that characterised the Cretaceous of the EGC. The earliest fill of the Buduq Trough is preserved in the east and is represented by Cenomanian - Turonian sandstones and conglomerates (Fig. 2) (Bochud et al, 2011). The nature of this transition varies across and within the Trough; with the Cenomanian-Turonian conformable with the Aptian-Albian at Mt. Kelevudag (Kopaevich et al. 2015) and sitting directly on Barremian at Khirt (Fig. 2, Fig. 3). The overlying Coniacian-Maastrichtian is represented by mixed siliciclastic-carbonate turbidites and is conformable with the Cenomanian-Turonian in the west. In the east, near Cek, the Cenomanian-Turonian is absent, with the Campanian directly overlying Aptian-Albian thin-bedded mudstones, submarine landslide deposits and predominantly siliciclastic turbidites (Fig. 2, Fig. 3). Upper Cretaceous oceanic red beds (CORBs) are also seen throughout the Upper Cretaceous sequence, particularly in the Coniacian – Campanian turbidites and marls, indicating periodically oxic deep-marine conditions (e.g. Hu et al. 2005).

Data and Methods

The data set comprises 23 sedimentary logs, totalling 500 m, collected across the Buduq Trough (see supplementary material). Logs were generally collected at 1:25 scale. Bedding and structural data (Fig. 4) and palaeocurrent data (Fig. 5) were collected to ground truth the geological map and cross sections of Bochud (2011). Palaeocurrent readings were quite rare and were taken only where sedimentary structures were clear enough to permit unambiguous data collection. Sparse biostratigraphic data (Bochud 2011) hinders precise correlation across the study area. Chrono-stratigraphic subdivision of the Buduq Trough are still being refined (cf. Bochud 2011; Bragina & Bragin, 2015; Kopaevich et al. 2015), possibly due to the litho-stratigraphic similarities between the units and the complex paleo-topography in which they were deposited (Egan et al. 2009). Therefore we use mapped stratigraphic units (J_1, J_2, K_1, K_2 etc.) and lithostratigraphy to suggest associated ages (Bochud 2011). Sedimentary logs were used to develop a lithofacies scheme (Fig. 6, Table 1) and facies associations (Fig. 7).

Over 10,000 sedimentological measurements (e.g. bed thickness, grain size, facies) were collected and quantitatively analysed (see supplementary material). Stratigraphic logs were assigned one of seven facies associations (Fig. 7) in order to quantitively compare bed statistics across deep-marine sub-environments (Fig. 8, 9, 10, 11).

Results

Lithofacies

Carbonate and siliciclastic lithofacies presented in Table 1 and Fig. 6 represent beds deposited by individual events (event beds) and are classified based on outcrop observations. 'Mud' is used here as a general term, for mixtures of clay, silt and organic fragments.

Facies Associations

Facies associations have been interpreted based on the dominant lithofacies (Fig. 6, Table 1) and architecture of a given succession and are subdivided into siliciclastic and mixed (carbonate and siliciclastic) associations (Fig. 7). Facies associations FA1, FA2 and FA3 are Cenomanian-Turonian and FA 4, FA 5, FA 6 and FA 7 are Coniacian-Maastrichitan (Bochud 2011). Facies associations commonly used for lobes (Prélat et al. 2009; Spychala et al. 2017) and channels (Kane & Hodgson, 2011; Hubbard et al. 2014) best fit our observations.

Siliciclastic Facies Associations

FA 1: Lobe Fringe
Observations: FA 1 is dominated by metre-scale packages of thin-bedded siliciclastic siltstones to fine-grained sandstones with subordinate mudstones and medium-bedded siliciclastic sandstones (Fig. 7A). Beds are laterally extensive for 100's of metres and are commonly flat based and flat topped, often showing normal-grading from fine sandstone to siltstone. Planar and convolute laminations are observed in the upper part of many beds. Debrites, hybrid beds, conglomerates and thick-bedded sandstones are absent.

Interpretations: Thin-bedded, structured sandstones are interpreted to be deposited from low-concentration turbidity currents (Mutti et al. 1992; Jobe et al. 2012; Talling et al. 2012). The lack of hybrid beds and the thin-bedded nature, lateral-extent, fine-grain size and lack of ripple-stratification indicate deposition in a distal lobe fringe (Fig. 9) (Mutti 1977; Prélat et al. 2009; Marini et al. 2015; Spychala et al, 2017).

FA 2: Channel Axis
Observations: FA 2 is composed of metre-scale thick-bedded medium-pebbly sandstones and conglomerates with lesser medium-bedded sandstones and rare thin-bedded sandstones, mudstones, debrites and hybrid beds (Fig. 7B). Within the Cenomanian-Turonian succession, FA 2 has the highest frequency of thick-bedded sandstones, conglomerates and bi-tripartite beds (Fig. 9). Conglomerates often grade normally into thick-bedded sandstones, commonly associated with a grain size break, with coarse-granular sandstone grade often missing. Where conglomerates do not grade into thick-bedded sandstones they are amalgamated or are less commonly separated by thin beds of mudstone. Conglomerates are poorly-sorted, clast-supported and contain sub-angular – sub-rounded clasts of limestone, sandstone and mudstone that often crudely grade from cobbles to pebbles upwards (Fig. 11). Conglomerates also often contain disarticulated shelly fragments. Sandstone and conglomerate bases are almost always erosional.

Thick-bedded sandstones are often normally-graded but can be non-graded or inversely-graded. Decimetre scale mud-clasts are common throughout thick-bedded sandstones and low angle cross-stratification is infrequently observed. Thin- to medium-bedded sandstones often have erosional bases and contain convolute, hummock-like and planar laminations and are normally-graded, with rare examples of inverse- or non- grading. These sandstones are either amalgamated or separated by 10 cm thick mudstone layers, and often contain mud-clasts throughout the bed with granules concentrated at the bed base. Sporadic debrites are also seen within FA 2; these have a deformed mudstone matrix and contain clasts of limestone and sandstone. Hybrid beds are amalgamated into 30-50 cm packages, with individual beds commonly consisting of a thin 2-4 cm fine-medium grained sandstone overlain by a clast and shelly fragment rich 8-12 cm muddy very fine sandstone debrite.
'Off-axis' successions have fewer thick-bedded sandstones and conglomerates than FA 2, but more than FA 3, and fewer thin-medium, thick-bedded sandstones than FA 3, but more than FA 2 (Fig. 9).

Interpretations: The thick-bedded nature, coarse grain size, amalgamation, erosion and entrainment of clasts within the sandstones suggests that the parent flows were highly energetic and capable of eroding and bypassing sediment (Mutti 1992; Stevenson et al. 2015) and are thus these beds are interpreted as high density turbidites (Lowe 1982). The poorly-sorted nature of the conglomerates suggests that they were initially deposited by laminar flows (Sohn 2000), however apparent grading of conglomerates into thick-bedded sandstones could reflect the transition of hyper-concentrated submarine debris flows into highly-concentrated turbulent flows (Mulder and Alexander, 2001) due to entrainment of ambient water (Postma et al. 1988; Kane et al. 2009).

The transition from conglomerates to medium-very coarse sandstone is associated with a grain size break, often missing the granule fraction, suggesting bypass of flow (Stevenson et al. 2015). The coarse-grain size and basal location of the conglomerates with respect to thick-bedded sandstones suggests these beds could have been deposited as channel-base lags (Hubbard et al. 2014). Erosionally-based lenticular sandstones grading from cobble- to fine-sandstones are interpreted to represent submarine channel fill (Jobe et al. 2017; Bell et al. 2018). This facies association is consistent with gravelly-conglomeratic deposits reported elsewhere to represent submarine channel axis deposition (Postma, 1984; Nemec & Steel 1984; Surlyk 1984; Dickie & Hein, 1995; Kane et al. 2009; Li et al. 2018; McArthur et al. 2019; Kneller et al. 2020).

While typically related to storm deposits (e.g. Hunter & Clifton, 1982), hummock-like cross-lamination have been interpreted in deep marine environments elsewhere as anti-dune stratification (Mulder et al. 2009), bottom current deposits (Basilici et al. 2012) and reworking of an initial deposit by a subsequent flow (Mutti 1992; Tinterri et al. 2017). The channel axis interpretation of FA 2 speculatively suggests anti-dunes formed by supercritical flows are the most probable interpretation of these hummock-like structures (Araya & Masuda, 2001; Alexander, 2008).

FA 3: Channel Margin

Observations: FA 3 comprises thin-medium bedded fine-granular sandstones in 30-80 cm packages interbedded with 10-90 cm dark mudstones (Fig. 7C). Within the siliciclastic Cenomanian-

Turonian succession FA 3 has the highest frequency of thin-medium bedded sandstones (Fig. 9). Conglomerates and thick-bedded sandstones are rare in FA 3 (Fig. 9). Thin-bedded sandstones and the upper part of medium-bedded sandstones can be argillaceous, with visible micaceous grains and are often planar, ripple and convolute laminated, with rarer hummock-like laminations. Sandstones are often normally-graded but inverse-grading is also observed. Beds of medium thickness are rich in mud-clasts and commonly amalgamated along mud-clast laden surfaces, bases can be highly erosive and scour-like, removing a significant proportion of the underlying bed. Thin-bedded sandstones can be flat or erosively-based, commonly scoured; where bases are erosional the lowermost part of the bed is commonly rich in granule-grade material (Fig. 7C). Granules and coarser fragments are composed of limestone and sandstone. Infrequent hybrid beds are composed of medium-coarse grained siliciclastic sandstone, overlain by a muddy, occasionally marly fine sandstone debrite.

Interpretations: The thin-bedded nature and presence of tractional structures indicate that this facies association was deposited by a low-density turbidity current (Lowe 1982). Presence of hummock-like laminations could indicate storm-wave influenced deposition (Harms et al. 1975), however their presence within a succession containing thick, dark mudstones and frequent sediment gravity flows suggests a deep-marine origin. Anti-dune formation (Mulder et al. 2009) and tractional reworking of an aggrading deposit (Mutti 1992; Tinterri et al. 2017; Bell et al. 2018) have both been interpreted to form similar hummock-like lamination in deep marine environments. Clean sandstones which grade into argillaceous, micaceous sandstones could indicate transitional flow deposits (Sylvester & Lowe 2004; Baas et al. 2009; Kane & Pontén 2012). The thin-bedded, coarse grain size and erosive nature of these deposits, along with the presence of supercritical bedforms, is similar to the overbank deposits seen adjacent to bypass-dominated channels (Kane & Hodgson 2011; Hubbard et al. 2014; Jobe et al. 2017, Lin et al. 2018, McArthur et al. 2019). These similarities, coupled with the along strike location of FA 3 adjacent to FA 2 (channel axis), has led to the interpretation of FA 3 as a channel overbank (Fig. 9). The lateral transition of FA 2 and 3 is indicative of 'on-axis' to 'off-axis' channel-belt facies (Kane et al. 2009).

FA 4: Lobe Axis

Observations: FA 4 is dominated by > 1 m thick packages of amalgamated conglomerates (Fig. 7D, Fig. 9) interbedded with thin-thick bedded very fine - very coarse sandstones. Within the Coniacian-Maastrichtian succession, the thickest conglomerates are found within FA4 (Fig. 8). The conglomerates are laterally discontinuous, erosionally-based, and are either flat-topped when onlapping, or convex-up when downlapping, the slope (Fig. 7, Fig. 12). Conglomerates increase in frequency, clast size (up to cobble-grade) and thickness, up stratigraphy (Fig. 8) and contain sub-angular to rounded clasts of limestone, sandstone and mudstone (Fig. 11). Within the Coniacian-Maastrichtian stratigraphy the greatest number of amalgamated beds is in FA4 (Fig. 10) and the largest grain size range (majority of beds between very-fine sandstone to medium grained sandstone) is observed (Fig. 8). Within FA 4, a coarser grain size class (of coarse grained sandstone or above) is observed which is almost absent in other Coniacian-Maastrichtian facies associations (FA 5, FA 6, FA 7) (Fig. 8).

Interpretations: Amalgamation of event beds suggests parent flows were energetic and capable of eroding sediment into the flow (Lowe 1982; Stevenson et al. 2015) and amalgamation of conglomerates indicates deposition in a debris-flow dominated environment (Surlyk 1984; Postma 1984; Dickie & Hein, 1995), similar to the debris flow dominated lobes described by McHargue et al. (2019). These conglomerates could also represent sediment bypass within lobe axes (e.g. Kane et al. 2009) or channel fill conglomerates (e.g. Knaust et al. 2014), however their thickness, stacking and geometry are most likely to represent deposition in the axis of a debris-flow dominated lobe.

Mixed Facies Associations

FA 5: Lobe Off-Axis

Observations: FA 5 is represented by erosively-based thin- to medium-bedded, fine-coarse grained siliciclastic sandstones and thin- to medium-bedded fine-grained calcareous siltstones, conglomerates and fine sandstones (Fig. 7E, Fig. 8). Sandstones with siliciclastic bases and calcareous tops are present throughout and are often amalgamated with siliciclastic and calcareous sandstones, forming packages separated by mudstones and silty-mudstones. Calcareous beds are typically flat-based when overlying mudstones, whilst siliciclastic beds are commonly erosive. Calcareous siltstones and sandstones are massive, whilst siliciclastic sandstones show planar, convolute and ripple laminations, but can also be structureless. Debrites are interspersed, often incorporating thin-bedded calcareous siltstones and sandstones. Hybrid beds are rare (Fig. 9).

Interpretations: The presence of both calcareous and siliciclastic sandstones suggests deposition in a mixed system (Fig. 1, Fig. 10) (Al-Mashaikie & Mohammed, 2017; Chiarella et al. 2017; Walker et al. 2019). Structureless medium-bedded calcareous siltstones and sandstones are interpreted to represent deposition from medium density turbidity currents (Kneller & Branney 1995; Talling et al. 2012; Soutter et al. 2019) aggrading quickly enough to prevent tractional sedimentary structure development in their basal divisions (Kneller & Branney 1995; Sumner et al. 2008). This depositional process is complicated within the calcareous medium-bedded deposits, which appear to have aggraded much more slowly than their siliciclastic counterparts, as evidenced by thin-bedded and medium-grained siliciclastic beds being deposited within medium-bedded and fine-grained calcareous beds. The presence of medium-density turbidites, relatively coarse grain size and common amalgamation suggests lobe off axis deposition (Prélat et al. 2009; Spychala et al. 2017).

FA 6: Proximal Fringe

Observations: Primarily composed of normally-graded, thin-medium bedded calcareous very-fine to fine-grained sandstones and siltstones, with subordinate thin-bedded siliciclastic fine-medium sandstones and mixed siliciclastic and calcareous sandstones (Fig. 7F, Fig. 8, Fig. 9). Calcareous siltstones and sandstones are flat based when overlying mudstones, but are often erosive at amalgamation surfaces (Fig. 10). Siliciclastic sandstones, either isolated or within mixed beds, are frequently < 3 cm thick, with flat to weakly erosive bases (Fig. 6). Debrites are interspersed within FA 6 and often rework the thin-bedded calcareous siltstones and sandstones. Planar laminations are common within the thin-bedded siliciclastic and calcareous sandstones. Less common ripple laminations show multiple and opposing palaeocurrent orientations. Hybrid beds are rare (Fig. 9).

Interpretations: The presence of both calcareous and siliciclastic sandstones suggests deposition in a mixed system (Fig. 1, Fig. 10) (Al-Mashaikie & Mohammed, 2017; Chiarella et al. 2017; Walker et al. 2019). Calcareous sandstones are interpreted to represent deposition from low- to medium-density turbidity currents based on their bed thickness, fine grain size and structuration (Fig. 9) (Lowe 1982; Mutti 1992). The thin-bedded siliciclastic sandstones could represent the depositional products of flow transformation from up-dip debris flows (i.e. the up-dip conglomerates) to turbulent flows following the entrainment of ambient water (Potsma 1988; Haughton et al. 2009), which punctuate slowly aggrading calcareous turbidites, interpreted to represent the remnants of dilute flows (Remacha & Fernández, 2003).

The preservation of both structured and structureless sandstones suggests an off-axis location of deposition; similar preservation of both deposit types has been interpreted in the proximal lobe fringe elsewhere (Prélat et al. 2009; Spychala et al. 2017; Soutter et al. 2019). FA 6 is differentiated from FA 5 based on its thinner beds and less frequent erosional events, and is therefore interpreted as being more distal and deposited within the proximal fringe. Hybrids beds are rare throughout the system therefore a distinction between frontal fringe and lateral fringe is difficult to decipher (e.g. Spychala et al. 2017).

FA 7: Distal Fringe

Observations: Dominated by laterally extensive, metre-scale packages of thin-bedded amalgamated calcareous sandstones which are normally-graded from very fine – fine sandstone to siltstone and are interbedded with metre-scale mudstones and silty-mudstones (Fig. 7G, Fig. 8, Fig. 9). Beds are flat-based, flat-topped and frequently contain both parallel and convolute laminations. Medium-bedded calcareous siltstones-fine sandstones are present, and may reflect amalgamated thinner-beds which are difficult to decipher. Debrites, siliciclastic thin-bedded sandstones and hybrid beds are rare (Fig. 9). The smallest grain size range (between siltstone and very-fine sandstone) is observed in FA6 and FA7 (Fig. 8) and amalgamation is infrequent (Fig. 10). More thin beds are seen in FA7 than elsewhere in stratigraphy (Fig. 7C, Fig. 8, Fig. 9).

Interpretations: Thin-bedded, structured sandstones are interpreted to be deposited from low-concentration turbidity currents (Mutti et al. 1992; Jobe et al. 2012; Talling et al. 2012). The presence of medium-bedded calcareous siltstones-fine sandstones and lack of ripple laminations suggest slow aggradation from a turbulent flow (Remacha & Fernández 2003; Bell et al. 2018). Lack of ripple lamination suggests flows did not reach significant velocity to generate ripple laminations (Baas et al. 2016). The infrequency of hybrid beds and siliciclastic beds within this facies association supports deposition within a carbonate dominated environment and the thin-bedded nature, lateral-extent, fine-grain size and lack of ripple-stratification suggests deposition in a distal lobe fringe (Mutti 1977; Prélat et al. 2009; Marini et al. 2015; Spychala et al, 2017).

Discussion

Nature of the Upper Cretaceous Topography

Toward the west of the Qonaqkend Zone, Upper Cretaceous deep-marine sandstones and limestones can be seen to thin towards, and onlap, Upper Jurassic limestones (Fig. 12, Fig. 13, Fig.

14). These Upper Jurassic limestones must therefore have formed 100s of metres of relief on the Cretaceous seafloor. The most likely mechanism for the generation of seafloor topography is an allochtonous block (Fig. 13, Fig. 14, Fig. 15). The presence of decametre-scale allochtonous blocks (mega-clasts of Blair & McPherson 1999) and submarine landslide deposits throughout the Cretaceous stratigraphy indicates a highly unstable margin, supporting this view (Fig. 13, Fig. 15). The identification of a basin-scale submarine landslide deposit, which forms the Qizilqaya and Shagdag mountains toward the west, further validates this interpretation (Bochud 2011) (Fig. 15) with the mega-clasts in the west possibly forming part of this deposit (Fig. 14, Fig. 15, Fig. 16). The contact is therefore formed as the Cretaceous stratigraphy infilled the accommodation present on the irregular surface of the deposit. Such relationships have been observed at outcrop (e.g. Burbank et al. 1992; Armitage et al. 2009, Kneller et al. 2018) and in the subsurface (Fig. 17) (e.g. Soutter et al. 2018, Casson et al. 2020). Differential compaction around these rigid blocks will have resulted in steepening of strata adjacent to the block, which may contribute to the gradual steepening identified (Fig. 12, Fig. 14), which has been reported elsewhere (e.g. Burbank et al. 1992).

Upper Cretaceous evolution of the Buduq Trough

Deep-marine deposition within the Buduq Trough began following a period of compression and folding in the mid-Cretaceous (Fig. 16) (Egan et al. 2009, Bochud 2011). Evidence of this compression is seen within the earliest fill in the Trough, which is preserved toward the east of the Qonaqkend structural zone. This early fill is represented by Cenomanian - Turonian conglomeratic slope channels that either erode into Barremian deep-marine mudstones or sit conformably on thin-bedded Aptian-Albian siliciclastic turbidites. These basal-Cenomanian stratigraphic relationships are suggested to be caused by channels preferentially infilling lows present on seafloor, forming entrenched channel axes that pinch-out laterally against Barremian mudstones (Fig. 16). These lows may have formed during mid-Cretaceous compression and folding (Egan et al. 2009; Sosson et al. 2016) or through submarine slope failure and consequent scour-formation.

It is possible that poorly preserved thin-bedded Aptian-Albian turbidites represent the distal extents of the Cenomanian slope channels that were either eroded by the channels during progradation or deposited within isolated lows on the Barremian slope. These lows may have formed in response to similar processes to those which entrenched the Cenomanian channels. The abrupt nature of the transition from distal fine-grained turbidite deposition to conglomeratic slope channels may correspond to either tectonic rejuvenation during the Mid-Cretaceous compressional event (Fig. 16) (Egan et al. 2009) and/or an abrupt relative sea-level fall, such as the eustatic sea-level fall seen in the mid-Cenomanian (Miller et al. 2003).

Evidence for basinal topography is present during deposition of the Cenomanian – Turonian, with the sequence almost entirely absent 10 km to the west at Cek, indicating the presence of a relative high in this location. Submarine landslide thicknesses also increase toward this high in the Barremian, suggesting the high influenced deposition from the Lower Cretaceous until the Turonian. Previous work has shown the presence of a large Lower Cretaceous submarine landslide toward the west (Fig. 16) (Bochud 2011), which is likely to form the high and the complex stratigraphic relationships described previously (Fig. 13, Fig. 14, Fig. 15). It is also likely that this submarine landslide, and other more minor ones in the area, were emplaced during an earlier period of tectonism and instability related to Lower Cretaceous compression (Fig. 16). Evidence for topography (Fig. 12) in the Late Cretaceous is also evident on a smaller scale through paleocurrent reversals in low-density turbidites (e.g. Kneller et al. 1991) indicating a northward-dipping slope confining southward-directed flows (Fig. 5, Fig. 12), and through the deposition of Upper Jurassic blocks within the Turonian succession, indicating slope instability during this period (Fig. 13, Fig. 15).

Following the Cenomanian-Turonian regression the Trough begins to deepen again during the Coniacian-Maastrichtian (CM), as represented by the deposition of laterally-extensive, thin- to medium-bedded, mixed-siliciclastic-carbonate turbidites overlying the slope channels (Fig. 16). The mixed-lithology of the turbidites contrasts with the dominantly siliciclastic Aptian-Albian turbidites underlying the slope channels, indicating a change in source or paleogeography between the Lower and Upper Cretaceous (Fig. 5, Fig. 16). The presence of thinning and facies changes toward present-day syncline margins, frequent debrites and out-runner blocks, and divergent palaeocurrent distributions indicates that basinal topography had an impact on CM deposition (Fig. 5, Fig. 12, Fig. 13, Fig. 15). This topography may have been formed by differential compaction over the rigid limestone mega-clast, or external compression (Fig. 14, Fig. 15, Fig. 16). Erosional contacts are seen within the CM succession at the base of small, metre-scale channel fills, which occur with increasing frequency through time. These small channel fills are filled by conglomerates and high-density turbidites with similar compositions to the underlying and much more extensive slope channels. The channels are therefore interpreted as small distributary channels in the axes of lobes that formed at the distal ends of the underlying slope channels (e.g. Normark et al. 1979). The increasing frequency and thickness of these conglomerates through the CM (Fig. 8) may therefore represent gradual progradation of the slope channels following their abrupt backstep at the end of the Turonian. Clasts within these younger conglomerates are also more limestone-dominated, which fits with the transition to a more carbonate-dominated system through the Upper Cretaceous (Fig. 11, Fig. 16, Fig. 18).

Mixed-deep-marine deposition continues in the Buduq Trough throughout the remainder of the Cretaceous until Palaeogene compression ceases deposition (Bochud 2011), forming an unconformity between the Upper Cretaceous and overlying Palaeogene and Neogene sediments (Fig. 2, Fig. 3).

A Subsurface Analogue for the Buduq Trough

A seismic-scale equivalent of a mixed-system analogous to the Cretaceous Buduq Trough has been identified and is used to support and increase the resolution of our outcrop-based model. The continental margin offshore The Gambia, NW Africa, developed through the Late Cretaceous with remarkable similarities in timing and evolution to the Buduq Trough (summarised in Casson et al. 2020 in press; Fig. 17). Unconfined mixed-systems developed on the deep-marine basin floor are interpreted to have been line-fed through a heavily canyonised unconformity surface (Fig. 17C). Seismic geomorphology reveals the interfingering of siliciclastic-dominated and carbonate-

dominated systems (i.e. at X and Y Fig. 19), similar to that observed on facies and facies architecture scale in the EGC (e.g. Fig. 6, Fig. 7).
Sediment gravity flows through the canyons eroded into the underlying carbonate platform redepositing hundreds of metre-scale, seismically-resolvable carbonate mega-clasts 20+ km from the escarpment (Fig. 17B, D); our field work suggests that these blocks may be associated with a multitude of different types and sizes of submarine landslides and blocks that are below seismic scale (Fig. 13, Fig. 15). The presence of carbonate blocks and lobe-architecture in the carbonate-dominated systems (*sensu* McHargue et al. 2019) suggests deposition by debris-flows (i.e. FA 4). Hence two stages of mixing occurs, firstly during erosion to form mixed lithology flows, and then through deposition of interfingering systems. Pervasively channelised siliciclastic-systems with single feeder channels show a distinct seismic geomorphological response to their carbonate counterparts (Fig. 17D, E). The lateral location along the margin of siliciclastic-dominated systems is conceivably related to sediment input points (i.e. shelf-incising canyons) capturing an extra-basinal source of siliciclastic sediment from the shallow marine environment, away from shelfal carbonate factories. Basin floor topography is created by early deposits and influences subsequent lobe deposition (Fig. 17), causing stacking and lateral migration of lobes, which cannot be resolved in the Buduq Trough (Fig. 18) probably because the scale of the study area is smaller than the scale at which migration occurred.

Documentation of ancient subsurface mixed-systems has been achieved from the interpretation of seismic reflection data (e.g. Moscardelli et al. 2019, Casson et al. 2020). It may also be possible that transitions from calcareous-dominated to siliciclastic-dominated deep-marine systems, which are commonly associated with the rapid arrival (progradation) of the siliciclastic system (e.g. Scott et al. 2010; Kilhams et al. 2012; 2015; Soutter et al. 2019; Cumberpatch et al. in prep.), may have been overlooked as 'transition zones', and in fact represent short-lived mixed systems, which are often below the scale of seismic resolution. The role of mixed-system interactions on a grain-scale and its implications in terms of reservoir quality remain unclear until such systems are drilled (Chiarella et al. 2017; Bell et al. 2018; Moscardelli et al. 2019).

Mixed lobes

Lobe sub-environments: If individually observed, the siliciclastic system within the mixed succession could be interpreted as stacked lobes with axial, off-axial and fringe sub-environments identified. The calcareous system, however, would be interpreted as being predominantly lobe fringe deposition (Remacha & Fernández 2003; Bell et al. 2018). Since the two systems are mixed it is difficult to assign a single lobe sub-environment to a sequence of beds as they represent the inter-fingering of two systems (Fig. 19). Due to the interaction of these systems, siliciclastic lobe elements are likely to occur within calcareous lobe elements (Fig. 1, Fig. 17, Fig. 19) (Prélat et al. 2009), forming stacks of mixed event beds (D, Table 1). This is further complicated by often highly erosive siliciclastic turbidity currents which can rework calcareous beds, as evidenced by calcareous rip-up clasts within siliciclastic turbidites. This may remove individual calcareous lobe elements from the rock record, and make stacking interpretations more difficult (Fig. 18) (Braga et al. 2001).

Due to these complexities it is perhaps necessary to refer to such systems with a more specific descriptor (e.g. mixed axis-fringe), or broadly refer to them as 'mixed systems' in order to allude to their complexity and contrast them from siliciclastic-dominated systems (Fig. 19). Use of the siliciclastic lobe hierarchy of Prélat et al. (2009) is possible in mixed systems, but calcareous and siliciclastic descriptors are required (Fig. 19). It is possible to decipher the different systems in our field and subsurface examples, due to their lithological differences being visually resolvable at outcrop (Fig. 6, Fig. 7) and showing different seismic characteristics in the subsurface (Fig. 17, Fig. 19). However, without detailed provenance and geochemical analysis it would be very difficult to decipher the mixing of two siliciclastic systems or two calcareous systems, due to similarity in depositional facies and thus seismic character. Unless an individual system can be followed from source to sink in outcrop or the subsurface we must always consider the possibility of multiple systems interacting, modulating each other and complicating stacking patterns (Fig. 19).

***Stacking patterns**:* Deep-marine stacking motifs can show either aggradational, progradational, retrogradational or unorganized stacking patterns (Stow & Mayall, 2000; Deptuck et al. 2007; Straub et al. 2009; Prélat & Hodgson 2013), which can be modulated by both external and internal processes (e.g. Ferguson et al. 2020). Our study shows that in mixed systems it can be difficult to decipher stacking patterns within each individual system due to the convolution of each system by the other (Fig. 18, Fig. 19). Bed thickness trends within the calcareous turbidites are difficult to decipher, possibly due to their narrow grain size range preventing the identification of thinner-beds, and amalgamation within thicker beds (Fig. 18).

Siliciclastic conglomerates become more frequent and thicker throughout the Coniacian-Maastrichtian, perhaps reflecting a progradation of the siliciclastic system (Fig. 8, Fig. 16). However, bed thickness and grain size analysis for the Coniacian-Maastrichtian do not show any thickness trends or stacking patterns within the calcareous or siliciclastic turbidites (Fig. 18). This suggests that in mixed systems it may therefore not be possible to describe the progradation or retrogradation of an individual system, and only possible to describe the relative ratio between the two; the apparent dominance of the mixed system (e.g. if siliciclastic (s) > carbonate (c) this could be due to progradation of s or by the retrogradation of c, both of which are controlled by a number of external and internal forcings).

On the scale of the outcrops (100s m), the calcareous turbidites appear to be sheet-like, while the siliciclastic turbidites show thickness variation, representing more typical channel and lobe geometries (e.g. Prélat et al. 2009). Conglomerates observed in the FA4 appear to be confined to isolated depocentres and pinch-out across meters - 10s of meters, indicating the presence of subtle topography (Fig. 12). This suggests the deposition of the conglomerates may have been controlled by depositional topography (compensational stacking) and that the underlying calcareous turbidites do exhibit subtle, long-wavelength thickness changes over a greater scale than observed at outcrop, influencing subsequent sediment routing. Alternatively, the thinning of conglomerates was due to the basinal topography present at this time, preventing these highly-concentrated flows running-out over great distances (Fig. 12).

Mixed-system origin: Previous work on mixed systems has correlated alternations in calcareous and siliciclastic turbidites to 3rd order sea level cycles (Yose & Heller, 1989; Miller & Heller, 1994); the alternations in the Buduq Trough are lower frequency than these cycles but could be interpreted as fifth-sixth order sea level cycles (parasequences) occurring on a 10,000 – 100,000 year cycle (Fig. 16) (Van Wagoner et al. 1990), related to Milankovitch orbital cycling (Goldhammer et al. 1990; D'Argenio et al. 1999). Elsewhere mixed systems have been interpreted to represent alternating cool-wet and cold-dry climate cycles driven by precession orbital cycles (García-García et al. 2009). No obvious stacking can be deduced in the study area (Fig. 18) preventing a confident interpretation to be made regarding the forcings behind the high-frequency lithological variations.

Rugose carbonate platform margins (e.g. Saller et al. 1989; Grant et al. 2019, Casson et al. 2020), like those observed in the Buduq Trough (Fig. 13, Fig. 16, Fig. 17), have been proposed as conduits for siliciclastics without requiring a sea level change (Francis et al. 2008; Braga et al. 2008; Puga-Bernabéu et al. 2014; Al-Mashaikie & Mohammed, 2017; Walker et al. 2019). This could indicate that the calcareous deep-marine system in the Buduq Trough is part of a much more extensive and line-fed system derived from shedding of active carbonate factories perched on the shelf (e.g. Fig. 17). The contemporaneous siliciclastic system may therefore have been derived from multiple point source conduits along this margin that either 1) periodically punctuated this larger carbonate system or 2) were long-lived conduits permanently bound by carbonate factories (Fig. 16) (Mueller et al. 2017; Moscardelli et al. 2019). Two different sources for separate components of a mixed system have been documented elsewhere (Fig. 1, Fig. 17, Fig. 19A) (Ditty et al. 1997; Riaz Ahmad & Jamil Afzal, 2012; Poprawski et al. 2014; 2016; Chiarella et al. 2017). The presence of Late Jurassic blocks (Fig. 13, Fig. 15) within the Cretaceous complicates this model, with the blocks interpreted as either 1) Late Cretaceous failures from an exposed Jurassic shelf, 2) out-running blocks from Lower Cretaceous failures (e.g. De Blasio et al. 2006) that were subsequently deposited around during the Late Cretaceous, or 3) blocks that were periodically shed through the Late Cretaceous from high-relief Lower Cretaceous slope submarine landslides identified in the west (Fig. 14, Fig. 16).

Palaeoflow indicators are limited for the calcareous system due to lack of ripple lamination developed in its fine-grained, slowly accumulating deposits (Baas et al. 2015). It is therefore difficult to decipher whether these siliciclastic and calcareous systems were perpendicular, oblique or parallel to each-other. The palaeoflow indicators that were collected, however, are consistent with a provenance to the north (Fig. 5, Fig. 12, Fig. 15) A northern provenance is also suggested from palaeographic maps for the interval, suggesting a Scythian platform source area (Nikishin et al. 1998), and unpublished provenance data (Vincent, pers.comm.).

Conclusion

This study uses the Upper Cretaceous Buduq Trough, Azerbaijan to document the characteristics of an unstable and mixed siliciclastic-carbonate system. Deposition in the Trough is represented by a Cenomanian-Turonian submarine channel complex, which transitions into a Coniacian-Maastrichtian mixed lobe succession. This sequence represents an abrupt Cenomanian regression, probably related to a mid-Cretaceous compressional event and/or an abrupt mid-Cenomanian eustatic sea level fall; followed by a relatively abrupt late Turonian-Coniacian transgression, likely associated with subsidence caused by back-arc extension. Throughout the remainder of the Cretaceous, the mixed-system exhibits weak progradation. A westerly topographic high formed by a Lower Cretaceous submarine landslide complex deposited during earlier compression is interpreted to have prevented deposition of the Cenomanian–Turonian toward the west. This submarine landslide complex may also have provided a lateral source for landslides through secondary remobilisation perpendicular to the regional palaeflow from the north. Bed pinch-out, thinning, ripple reflections and debrites provide further evidence for the presence of basinal topography during deposition.

The Coniacian-Maastrichtian mixed siliciclastic-calcareous deep marine system contains both siliciclastic and calcareous lobe elements, which represent different lobe sub-environments, requiring modification of terminology developed for siliciclastic lobes. Mixed systems are also shown to have unique facies, both in outcrop and a subsurface analogue from offshore The Gambia, reflecting differing depositional processes between the systems operating contemporaneously. Interaction between the two deep-marine environments characterising the mixed systems has also made stacking patterns difficult to decipher, with each system attenuating the other.

Acknowledgments

We are grateful to CASP for awarding a fieldwork grant for this project, to Chris Van Baak, Steve Vincent, Rashad Gulmammadov for their logistical support and to Muslim Gazibayov for his hospitality. Nigel Mountney is thanked for suggesting this study area in 2010. TGS are thanked for permission to publish the seismic data

Table 1:Summary of observations and interpretations of lithofacies, used to create facies associations

Facies	Description	Interpretation
Conglomerates (A)	0.1 to 3 + m thick beds of poorly-sorted, disorganised conglomerates. Most commonly clast-supported consisting of sub-angular to sub-rounded boulder-, cobble- and pebble-sized clasts of limestone and sandstone. Matrix comprises a poorly-sorted mix of all finer size fractions. Cm- 10cms scale mud-clasts occur sporadically throughout the beds. Bed bases are often erosive, and can be amalgamated. This facies often grades into thick bedded sandstones (C).	The characteristics of this facies suggest deposition from debris flows having cohesive as well as frictional strength (Fisher, 1971; Nemeck & Steel, 1984). The grading of conglomerates into thick-bedded sandstones reflects the transition of hyperconcentrated submarine debris flows into highly-concentrated turbulent flows (Mulder & Alexander, 2001; Sohn et al. 2002), due to the entrainment of ambient water (Postma et al. 1988).
Poorly sorted clast rich deposit (B)	0.1 – 1+ m thick poorly sorted deformed, matrix-supported units. Matrix can range from mudstone to coarse sandstone, and is often poorly-sorted and sheared. Clasts include cm-m scale limestone and sandstone blocks, rafts of remobilised folded thin-bedded sandstones, sporadic pebbles and granules and frequent mud-clasts. These deposits are commonly non-graded, but can show weak normal-grading.	The poorly-sorted matrix and large clast sizes are suggestive of 'flow freezing' of a flow with yield strength (Inverson et al. 2010), indicating 'en masse' deposition from a laminar flow (Nardin et al. 1979; Inverson 1997; Sohn 2000). Remobilised thin-bedded sandstones and intra-basinal clasts indicate localised mass failure and reworking.
Thick-bedded sandstones (C)	0.5 – 1+ m brown siliciclastic fine-granular sandstones. Normally-graded or non-graded and typically lacking in primary depositional structures. Bases are often sharp and erosive. Parallel laminations are sometimes present at bed tops and mud-clasts can be observed throughout. Weak cross-lamination is infrequently observed.	The general massive structuration of these deposits suggests that they represent rapid aggradation beneath a highly concentrated but dominantly turbulent flow, and are thus interpreted as high density turbidites (Lowe, 1982; Mutti 1992; Kneller & Branney 1995).
Mixed siliciclastic and calcareous sandstones (D)	0.1-1m beds of medium-bedded calcareous sandstones with punctuated interbeds of cm-scale thin-bedded siliciclastic sandstone, either as continuous beds or lenses. The medium-bedded calcareous sandstones are massive and the siliciclastic beds are often erosively-based and show tractional structures (ripple and planar lamination). Siliciclastic beds can be amalgamated with each other or isolated between calcareous siltstones or sandstones.	Medium-bedded calcareous sandstones are interpreted to represent deposition from a slowly aggrading dilute turbidity current. Periodic, thin-bedded siliciclastic sandstones represent deposition from a relatively quickly aggrading dilute turbidity current, which interacted with a much slower aggrading calcareous turbidity current.
Medium-bedded calcareous sandstones (E)	0.1-1 m thick beige beds of calcareous siltstone -fine sandstone. Normally-graded or non-graded. Planar lamination may be present, but other tractional structures are rare. Beds can be amalgamated.	Based on their tractional structures and normal-grading, beds are interpreted as having being deposited from dilute turbidity currents. These beds are interpreted as medium-density turbidites, due to larger bed thickness and infrequent tractional structures, than thin-bedded calcareous sandstones (G). Thicker beds and fine grain size indicate a slowly aggrading dilute turbidity current.
Medium-bedded siliciclastic sandstones (F)	0.1 -0.5 m thick brown beds of very fine – granular grained, commonly normally-graded, sandstones. Inverse-grading is infrequently observed. Basal parts of the bed are often structureless containing infrequent cm-scale mud-clasts while tops are rich in tractional structures including parallel, ripple and hummock-like laminations. Bed bases are often erosive, and can be amalgamated.	Based on their tractional structures and normal-grading, beds of this lithofacies are interpreted as deposition from a dilute turbidity current. These beds are interpreted as medium-density turbidites due to their bed thickness and common lack of structures in the lower part of the bed (e.g. Soutter et al. 2019).

Thin-bedded calcareous sandstones (G)	0.01 – 0.1 m thick beige beds of calcareous siltstone-fine sandstones. Can be normally-graded, often into silty-mudstones, or not graded. Planar laminations are observed but other tractional structures are typically absent. Individual beds are often amalgamated.	Thin-beds, fine grain size and weak planar laminations represent deposition from a low-concentration turbidity current (Mutti 1992; Jobe et al. 2012; Talling et al. 2012), indicating these beds are low-density turbidites. Fine grain size, thicker beds compared to thin-bedded siliciclastic sandstone (H) and absence of ripple laminations suggest slowly aggrading, dilute remnants of a turbulent flow, (Remacha & Fernández 2003; Bell et al. 2018), which did not reach significant velocity to generate ripple laminations (Baas et al. 2016).
Thin-bedded siliciclastic sandstones (H)	0.005 – 0.1 m thick brown beds of siliciclastic very fine- granular sandstones. Commonly normally-graded, occasional inverse-graded. Tractional structures (planar, ripple, hummock-like and convolute laminations) and sporadic mud-clasts are observed. Bases can be flat or weakly erosive and sometimes contain granules. Bed tops are often flat. Where present, ripples can show opposing palaeoflow.	Thin-bedded, structured sandstones are interpreted to be deposited from low-concentration turbidity currents (Mutti 1992; Jobe et al. 2012; Talling et al. 2012) and are therefore interpreted as low-density turbidites. Ripples with opposing palaeoflow suggests topographic interference.
Bi or tri-partite beds (I)	0.05-0.5 m thick beds that contain multiple parts. Typically consisting of a lower fine-coarse sandstone (division 1) overlain by a poorly-sorted muddy siltstone – medium sandstone (division 2). Division 3 is sometimes present consisting of a siltstone-fine grained sandstone loaded into division 2. Divisions 1 and 3 sometimes contain planar laminations and sporadic cm scale mud-clasts. Division 2 is often highly deformed and rich in mud-clasts and very coarse sandstone to pebble-grade clasts.	Tractional structures in division 1 and 3 indicate formation under turbulent flows. Poor-sorting and mud content suggest division 2 was deposited under a transitional-laminar flow regime. These bi-tri partite beds are hybrid beds (Haughton et al. 2009), generated by flow transformation from turbulent to laminar. Such transformation occurs through flow deceleration (Barker et al. 2008; Patacci et al. 2014) and by an increase in concentration of fines during flow run-out (Kane et al. 2017).
Mudstone (J)	0.005 – 8 m thick pale grey or red mudstone – fine siltstone beds, which are friable and often inferred in areas of missing section. Planar laminations, discontinuous drapes and lenses of siltstone may be present. Commonly calcareous in composition. Red beds are common at the base of the Campanian.	Low energy conditions, representative of background sedimentation via suspension fallout. Laminations may be present below the scale visible in outcrop, representing deposition from a dilute turbidity current (Boulesteix et al. 2019). Pale colour indicates low total organic carbon (TOC). Red beds are similar to Cretaceous Oceanic Red Beds (CORBS) described across Europe (Wang et al. 2005; Hu et al. 2005; Wagreich & Krenmayr, 2005) and represent deposition below the carbonate compensation depth (CCD) in a deep oceanic basin.

References

AHMAD, R. & AFZAL, J. (2012) Sequence Stratigraphy of the Mixed Carbonate-Siliciclastic System of the Eocene Nisai Formation, Pishin Basin. Distribution of Source Rocks and Reservoir Facies.

AL-MASHAIKIE, S. & Mohammed, Y. (2017) Anatomy of carbonate breccias, turbidite facies and depositional systems of Gercus Formation, in Donkan Area, Northern Iraq.

ALEXANDER, J. (2008) Bedforms in Froude-supercritcal flow. Marine and River Dune Dynamics.

ARAYA, T. & MASUDA, F. (2001) Sedimentary structures of antidunes: An overview. Journal of the Sedimentological Society of Japan, 53, 1-15.

ARMITAGE, D.A., ROMANS, B.W., COVAULT, J.A. & GRAHAM, S.A. (2009) The influence of mass-transport-deposit surface topography on the evolution of turbidite architecture: The Sierra Contreras, Tres Pasos Formation (Cretaceous), southern Chile. Journal of Sedimentary Research, 79(5), 287-301.

BAAS, J.H., BEST, J.L., PEAKALL, J. & WANG, M. (2009) A phase diagram for turbulent, transitional and laminar clay suspension flows. Journal of Sedimentary Research, 79, 162-183.

BAAS, J., BEST, J. & PEAKALL, J. (2016) Predicting bedforms and primary current stratification in cohesive mixtures of mud and sand. Journal of the Geological Society, 173(1), 12-45.

BARKER, S.P., HAUGHTON, P.D.W., MCCAFFREY, W.D., ARCHER, S.G. & HAKES, B. (2008). Development of rheological heterogeneity in clay-rich high-density turbidity currents: Aptian Britannia Sandstone Member, UK continental shelf. Journal of Sedimentary Research, 78, 45–68.

BASILICI, G., VIEIRA DE LUCA, P. H. & POIRÉ, D. G. (2012) Hummocky cross-stratification-like structures and combined-flow reipples in the Punta Negra Formation (Lower-Middle Devonian, Argentine Precordillera): A turbiditic deep-marine or storm-dominated prodelta inner-shelf systems?. Sedimentary Geology, 267-268, 73-92.

BELL, D., STEVENSON, C.J., KANE, I.A., HODGSON, D.M. & POYATOS-MORÉ, M. (2018) Topographic Controls On the Development of Contemporaneous but Contrasting Basin-Floor Depositional Architectures. Journal of Sedimentary Research, 88(10), 1166-1189.

BELL, D., KANE, I., PONTÉN, A., FLINT, S., HODGSON, D. & BARRETT, B. (2018) Spatial variability in depositional reservoir quality of deep-marine channel-fill and lobe deposits. Marine and Petroleum Geology, 98, 97-115.

BLAIR, T.C. & MCPHERSON J.G. (1999) Grain-size and textural classification of coarse sedimentary particles. Journal of Sedimentary Research, 69 (1), 6-19.

BOCHUD, M. (2011) Tectonics of the Eastern Greater Caucasus in Azerbaijan (Doctoral Dissertation, University of Freiburg). p. 202.

BOULESTEIX, K., POYATOS-MORE, M., FLINT, S.S, TAYLOR, K.G., HODGSON, D.M. AND HASIOTIS, S.T. (2019) Transport and Deposition of Mud in Deep-marine Environments: Processes and Stratigraphic Implications. Sedimentology, 66 (7), 2894-2925.

BOUMA, A.H. (1962) Sedimentology of some flysch deposits: a graphic approach to facies interpretation. Amsterdam, Elsevier, 168

BRAGA, J., MARTIN, J. & WOOD, J. (2001) Submarine lobes and feeder channels of redeposited,temperate carbonate and mixed siliciclastic-carbonate platform deposits (Vera Basin, Almeria, southern Spain). Sedimentology v. 48(1), 99-116.

BRAGINA, L. G. & BRAGIN, N.Y. (2015) New data on Albian-Coniacian radiolarians from the Kelevudag section (northeastern Azerbaijan). Stratigraphy and Geological Correlation, 23 (1), 45-56.

BROOKS, H.L., HODGSON, D.M., BRUNT, R.L., PEAKALL, J. & FLINT, S.S. (2018) Exhumed lateral margins and increasing flow confinement of a submarine landslide complex. Sedimentology, 65(4), 1067-1096.

BRUNET M. F., KOROTAEV M.V., ERSHOV A.V. & NIKISHIN A.M. (2003) The South Caspian Basin: a review of its evolution from subsidence modelling. Sedimentary Geology, 156 (1-4), 119-148.

BULL, S., CARTWRIGHT, J. & HUUSE, M. 2009. A review of kinematic indicators from mass-transport complexes using 3D seismic data. Marine and Petroleum Geology, 26(7), 1132-1151.

BURBANK, D.W., VERGÉS, J., MUNOZ, A. & BENTHAM, P. (1992) Coeval hindward- and forward-imbricating thrusting in the south-central Pyrenees, Spain: Timing and rates of shortening and deposition. Geological Society of America Bulletin, 104, 3-17.

CASSON, M.A., CALVÈS, G., REDFERN, J., HUUSE, M. & SAYERS, B. (2020) *in press.* Cretaceous continental margin evolution from quantitative seismic geomorphology, offshore NW Africa. Basin Research.

CHIARELLA, D., LONGHITANO, S.G. & TROPEANO, M. (2017). Types of mixing and heterogeneities in siliciclastic-carbonate sediments. Marine and Petroleum Geology, 88, 617-627.

CREVELLO, P.D. & SCHLAGER, W. (1980). Carbonate debris sheets and turbidites, Exuma Sound, Bahamas. Journal of Sedimentary Research, 50(4), 1121-1147.

CURRAY, J.R. & MOORE, D.G. (1971) Growth of the Bengal deep-sea fan and denudation in the Himalayas. Geological Society of America Bulletin, 82(3), 563-572.

D'ARGENIO, B., FERRERI, V., RASPINI, A., AMODIO, S. & BUONOCUNTO, F. 1999. Cyclostratigraphy of a carbonate platform as a tool for high-precision correlation. Tectonophysics, 315(1-4), 357-384.

DEPTUCK, M.E., SYLVESTER, Z., PIRMEZ, C. & O'BYRNE, C. (2007). Migration-aggradation history and 3-D seismic geomorphology of submarine channels in the Pleistocene Benin-major Canyon, western Niger Delta slope. Marine and Petroleum Geology, 24 (6-9), 406-433.

DE BLASIO, F.V., ENGVIK, L.E. & ELVERHØI, A. (2006) Sliding of outrunner blocks from submarine landslides. Geophysical Research Letters, 33(6).

DICKIE, J. & HEIN, F. (1995) Conglomeratic fan deltas and submarine fans of the Jurassic Laberge Group, Whitehorse Trough, Yukon Territory, Canada: fore-arc sedimentation and unroofing of a volcanic island arc complex. Sedimentary Geology, 98(1-4), 263-292.

DITTY, P.S., HARMON, C.J., PILKEY, O.H., BALL, M.M. & RICHARDSON, E.S. (1977) Mixed terrigenous—Carbonate sedimentation in the Hispaniola—Caicos turbidite basin. Marine Geology, 24(1), 1-20.

DORSEY, R.J. & KIDWELL, S.M. (1999) Mixed carbonate-siliciclastic sedimentation on a tectonically active margin: Example from the Pliocene of Baja California Sur, Mexico. Geology, 27(10), 935-938.

DUNBAR, G.B. & DICKENS, G.R. (2003) Late Quaternary shedding of shallow-marine carbonate along a tropical mixed siliciclastic–carbonate shelf: Great Barrier Reef, Australia. Sedimentology, 50(6), 1061-1077.

EGAN, S.S., MOSAR, J., BRUNET, M.F. & KANGARLI, T. (2009) Subsidence and uplift mechanisms within the South Caspian Basin: insights from the onshore and offshore Azerbaijan region. Geological Society, London, Special Publications, 312(1), 219-240.

FALLGATTER, C., KNELLER, B., PAIM, P.S. & MILANA, J.P. (2017) Transformation, partitioning and flow–deposit interactions during the run-out of megaflows: Sedimentology, 64(2), 359-387.

FERGUSON, R.A., KANE, I.A., EGGENHUISEN, J.T., POHL, F., TILSTON, M., SPYCHALA, Y.T. & BRUNT, R.L. (2020) Entangled external and internal controls on submarine fan evolution: an experimental perspective: The Depositional Record, in review.

FILDANI, A., CLARK, J., COVAULT, J.A., POWER, B., ROMANS, B. W. & AIELLO, I. W. (2018) Muddy sand and sandy mud on the distal Mississippi fan: Implications for lobe depositional processes: Geosphere, 14(3), 1051-1066.

FISHER, R.V. (1971) Features of coarse-grained, high concentration fluids and their deposits: Journal of Sedimentary Petrology, 41, 916- 927.

FONNESU, M., FELLETTI, F., HAUGHTON, P.D., PATACCI, M. & MCCAFFREY, W.D. (2018) Hybrid event bed character and distribution linked to turbidite system sub-environments: The North Apennine Gottero Sandstone (north-west Italy). Sedimentology, 65(1), 151-190.

FRANCIS, J., DANIELL, J., DROXLER, A., DICKENS, G., BENTLEY, S., PETERSON, L. BRADLEY, N. & BEAUFORT, L. (2008) Deep water geomorphology of the mixed siliciclastic-carbonate system, Gulf of Papua: Journal of Geophysical Research: Earth Surface, 113(1).

GARCÍA-GARCÍA, F., SORIA, J., SAR VISERAS, C. & FERNÁNDEZ, J. (2009) High-frequency rhythmicity in a mixed siliciclastic-carbonate shelf (Late Miocene, Guadix Basin, Spain): A model of interplay between climatic oscillations, subsidence and sediment dispersal. Journal of Sedimentary Research, 79, 302-315.

GAWTHORPE, R.L. (1986) Sedimentation during carbonate ramp-to-slope evolution in a tectonically active area: Bowland Basin (Dinantian), northern England: Sedimentology, 33(2), 185-206.

GEE, M.J.R., UY, H.S., WARREN, J., MORLEY, C.K. & LAMBIASE, J.J. (2007) The Brunei slide: a giant submarine landslide on the North West Borneo Margin revealed by 3D seismic data. Marine Geology, 246(1), 9-23.

GEORGIOPOULOU, A., MASSON, D.G., WYNN, R.B. & KRASTEL, S. (2010) Sahara Slide: Age, initiation, and processes of a giant submarine slide. Geochemistry, Geophysics, Geosystems, 11(7).

GOLDHAMMER, R.K., DUNN, P.A. & HARDIE, L.A. (1990) Depositional cycles, composite sea level changes, cycle stacking patterns, and the hierarchy of stratigraphic forcing - examples from platform carbonates of the Alpine Triassic. Geological Society of America Bulletin, 102, 535-562.

GOLONKA, J. 2004. Plate tectonic evolution of the southern margin of Eurasia in the Mesozoic and Cenozoic. Tectonophysics, 381(1-4), 235-273.

GRANT, R., UNDERHILL, J., HERNÁNDEZ-CASADO, J., BARKER, S. & JAMIESON, R. (2019) Upper Permian Zechstein Supergroup carbonate-evaporite platform palaeomorphology in the UK Southern North Sea. Marine and Petroleum Geology, 100, 484-518.

HAUGHTON, P.D.W., DAVIS, C., MCCAFFREY, W. & BARKER, S. (2009) Hybrid sediment gravity flow deposits - Classification, origin and significance. Marine and Petroleum Geology, 26, 1900-1918.

HU, X., JANSA, L., WANG, C., SARTI, M., BAK, K., WAGREICH, M., MICHALIK, J. & SOTAK, J. (2005) Upper Cretaceous oceanic red beds (CORBs) in the Tethys: occurrences, lithofacies, age, and environments. Cretaceous Research, 26(1), 3-20.

HARMS, J., SOUTHARD, J., SPEARING, D., & WALKER, R. (1975). Depositional Environments as Interpreted from Primary Sedimentary and Stratigraphic Sequences. SEPM.

HESSLER, A.M. & FILDANI, A. (2019) Deep-sea fans: tapping into Earth's changing landscapes. Journal of Sedimentary Research, 89(11), 1171-1179.

HUBBARD, S.M., COVAULT, J.A., FILDANI, A. & ROMANS, B.W. (2014) Sediment transfer and deposition in slope channels: Deciphering the record of enigmatic deep-sea processes from outcrop. Geological Society of America Bulletin, 126, 857-871.

HUNTER, R.E. & CLIFTON, E.H. (1982) Cyclic deposits and hummocky cross-stratification of probable storm origin in Upper Cretaceous rocks of the Cape Sebastian area, southwestern Oregon. Journal of Sedimentary Research, 52(1), 127-143.

ILSTAD, T., DE BLASIO, F.V., ELVERHØI, A., HARBITZ, C.B., ENGVIK, L., LONGVA, O. & MARR, J.G. (2004) On the frontal dynamics and morphology of submarine debris flows. Marine Geology, 213(1-4), 481-497.

INVERSON, R.M. (1997) The physics of debris flows. Reviews of Geophysics, 35, 245-296.

INVERSON, R.M., LOGAN, M., LAHUSEN, R.G. & BERTI, M. (2010) The perfect debris flow? Aggregated results from 28 largescale experiments. Journal of Geophysical Research: Earth Surface, 115, 1-29.

JACKSON, C.A-L. (2011) Three-dimensional seismic analysis of megaclast deformation within a mass transport deposit; implications for debris flow kinematics. Geology, 39(3), 203-206.

JOBE, Z.R., LOWE, D.R. & MORRIS, W.R. (2012) Climbing-ripple successions in turbidite systems: depositional environments, sedimentation and accumulation times. Sedimentology, 59, 867-898.

JOBE, Z.R., SYLVESTER, Z., HOWES, N., PIRMEZ, C., PARKER, A., CANTELLI, A., SMITH, R., WOLINKSKY, M.A., O'BRYNE, C., SLOWEY, N. & PRATHER, B. (2017) High-resolution, millennial-scale patterns of bed compensation on a sand-rich intraslope submarine fan, western Niger Delta slope. GSA Bulletin, 129, 23-37.

JOHNSON, A.M. (1970) Physical Processes in Geology. San Francisco: Freeman, Cooper and Company.

KANE, I.A. & HODGSON, D.M. (2011) Sedimentological criteria to differentiate submarine channel levee subenvironments: Exhumed examples from the Rosario Fm. (Upper Cretaceous) of Baja California, Mexico, and the Fort Brown Fm. (Permian), Karoo Basin, S. Africa. Marine and Petroleum Geology, 28, 807-823.

KANE, I.A., PONTÉN, A.S., VANGDAL, B., EGGENHUISEN, J.T., HODGSON, D.M. & SPYCHALA, Y.T. (2017) The stratigraphic record and processes of turbidity current transformation across deep-marine lobes. Sedimentology, 64(5), 1236-1273.

KANE, I.A. & PONTÉN, A.S.M. (2012) Submarine transitional flow deposits in the Paleogene Gulf of Mexico. Geology, 40, 1119–1122.

KANE, I.A., MCCAFFREY, W.D. & MARTINSEN, O.J. (2009) Allogenic vs. Autogenic Controls on Megaflute Formation. Journal of Sedimentary Research, v. 9, 643-651.

KANE, I.A., DYKSTRA, M.L., KNELLER, B.C., TREMBLAY, S. & MCCAFFREY, W.D. (2009) Architecture of coarse-grained channel-levée system: the Rosario Formation, Baja California, Mexico. Sedimentology, 56 (7), 2207-2234.

KILHAMS, B., HARTLEY, A., HUUSE, M. & DAVIS, C. (2012) Characterizing the Paleocene turbidites of the North Sea: The Mey Sandstone Member, Lista Formation, UK Central Graben. Petroleum Geoscience, 18(3), 337-354.

KILHAMS, B., HARTLEY, A., HUUSE, M. & DAVIS, C. (2015) Characterizing the Paleocene turbidites of the North Sea: Maureen formation, UK Central Graben. Geological Society Special Publication, 403, 43-62.

KNAUST, D., WARCHOL, M. & KANE, I.A. (2014) Ichnodiversity and ichnoabundance: revealing depositional trends in a confined turbidite system. Sedimentology, 61 (7), 2218-2267.

KNELLER, B. C. & BRANNEY, M.J. (1995) Sustained high-density turbidity currents and the deposition of thick massive sands. Sedimentology, 42, 607-616.

KNELLER, B., EDWARDS, D., MCCAFFREY, W. & MOORE, R. (1991) Oblique reflection of turbidity currents. Geology, 19(3), 250-252.

KNELLER, B., BOZETTI, G., CALLOW, R., DYKSTRA, M., HANSEN, L., KANE, I., LI, P., MCARTHUR, A., CATHARINA, A.S., SANTOS, T.D. & THOMPSON, P (2020) Architecture, process, and environmental diversity in a late Cretaceous slope channel system. Journal of Sedimentary Research, 90, 1-26.

KOPAEVICH, L.F., BENIAMOVSKII, V.N. & BRAGINA, L.G. (2015) Upper Albian-Turonian foraminifers and radiolarians from the Kelevudag section, northeastern Azerbaijan. Stratigraphy and Geological Correlation, 23(6), 580-599.

LI, P., KNELLER, B.C., THOMPSON, P., BOZETTI, G. & DOS SANTOS, T. (2018) Architectural and facies organisation of slope channel fills: Upper Cretaceous Rosario Formation, Baja California, Mexico. Marine and Petroleum Geology, 92, 632–649.

LOWE, D.R. (1982) Sediment gravity flows: Depositional models with special reference to the deposits of high-density turbidity currents. Journal of Sedimentary Research, 52, 279-297.

MARINI, M., MILLI, S., RAVNAS, R. & MOSCATELLI, M. (2015) A comparative study of confined vs. semi-confined turbidite lobes from the Lower Messinian Laga Basin (Central Apennines, Italy): implications for assessment of reservoir architecture. Marine and Petroleum Geology, 63, 142–165.

MCARTHUR, A., KANE, I., BOZETTI, G., HANSEN, L. & KNELLER, B. (2019) Supercritical flows overspilling from bypass-dominated submarine channels and the development of overbank bedforms: The Depositional Record.

MCHARGUE, T. R., HODGSON, D. M. & SHELEF, E. (2019) Architectural Diversity of Submarine Lobes. EarthArXiv.

MILLER, R.P. & HELLER, P.L. (1994) Depositional framework and controls on mixed carbonate-siliciclastic gravity flows: Pennsylvanian-Permian shelf to basin transect, south-western Great Basin, USA. Sedimentology, 41(1), 1-20.

MILLER, K.G., SUGARMAN, P.J., BROWNING, J.V., KOMINZ, M.A., HERNÁNDEZ, J.C., OLSSON, R.K., WRIGHT, J.D., FEIGENSON, M.D. & VAN SICKEL, W. (2003) Late Cretaceous chronology of large, rapid sea-level changes: Glacioeustasy during the greenhouse world. Geology, 31(7), 585-588.

MITCHELL, S.F., PICKERILL, R.K. & STEMANN, T.A. (2001) The Port Morant Formation (Upper Pleistocene, Jamaica): high resolution sedimentology and paleoenvironmental analysis of a mixed carbonate clastic lagoonal succession. Sedimentary Geology, 144(3-4), 291-306.

MOSCARDELLI, L., OCHOA, J., LUNT, I. & ZAHM, L. (2019) Mixed siliciclastic–carbonate systems and their impact for the development of deep-marine turbidites in continental margins: A case study from the Late Jurassic to Early Cretaceous Shelburne subbasin in offshore Nova Scotia. AAPG Bulletin, 103(10), 2487-2520.

MOUNT, J.F. (1984) Mixing of siliciclastic and carbonate sediments in shallow shelf environments. Geology, 12, 432-435.

MULDER, T. & ALEXANDER, J. (2001) Abrupt change in slope causes variation in the deposit thickness of concentrated particle-driven density currents. Marine Geology, 175(1-4), 221-235.

MULDER, T., ZARAGOSI, S., RAZIN, P., GRELAUD, C., LANFUMEY, V. & BAVOIL, F. (2009) A new conceptual model for the deposition process of homogenite: Application to a cretaceous megaturbidite of the western Pyrenees (Basque region, SW France). Sedimentary Geology, 222(3-4), 263-273.

MUELLER, P., PATACCI, M. & DI GIULIO, A. (2017) Hybrid event beds in the proximal to distal extensive lobe domain of the coarse-grained and sand-rich Bordighera turbidite system (NW Italy). Marine and Petroleum Geology, 86, 908-931.

MUTTI, E. (1977) Distinctive thin-bedded turbidite facies and related depositional environments in the Eocene Hecho Group (South-central Pyrenees, Spain). Sedimentology, 24, 107–131.

MUTTI, E. (1983) The Hecho Eocene submarine fan system, south-central Pyrenees, Spain. GeoMarine Letters, 3(2-4), 199-202.

MUTTI, E. (1992) Turbidite sandstones: AGIP- Instituto di Geologia, Università di Parma, p. 275.

NARDIN, T.R., HEIN, F.J., GORSLINE, D.S. & EDWARDS, B.D. (1979) A review of mass movement processes, sediment and acoustic characteristics, and contrasts in slope and base-of-slope systems versus canyon-fan-basin floor systems. SEPM Special Publications, 27, 61-73.

NEMEC, W. & STEEL, R.J. (1984) Alluvial and Coastal Conglomerates: Their Significant Features and Some Comments on Gravelly Mass-Flow Deposits.

NIKISHIN, A.M., CLOETINGH, S., BRUNET, M-F., STEPHENSON, R.A., BOLOTOV, S.N. & ERSHOV, A.V. (1998). Scythian Platform, Caucasus and Black Sea region: Mesozoic-Cenozoic tectonic history and dynamics. In: Peri-Tethys Memoir 3: stratigraphy and evolution of Peri-Tethyan platforms (Ed. by Crasquin-Soleau, S. and Barrier, É.) Mémoires du Muséum national d'Histoire naturelle, Paris, 177, 163-176.

NIKISHIN A.M., ZIEGLER P., PANOV, D.I., NAZAREVICH B.P., BRUNET M., F., STEPHENSON R.A., BOLOTOV S.N., KORATAEV M.V. & TIKHOMROV P.L. (2001) Mesozoic and Cainozoic evolution of the Scythian Platform - Black Sea - Caucasus domain. In: Peri-Tethys Memoir 6 - Peri-Tethyan rift/wrench basins and passive margins (Ed. by Ziegler P., Cavazza W., Robertson A.H.F. & Crasquin-Soleau S.), Mémoires du Muséum national d'Histoire naturelle, Paris, 186, 295-346.

NISSEN, S.E., HASKELL, N.L., STEINER, C.T. & COTERILL, K.L. (1999) Debris flow outrunner blocks, glide tracks, and pressure ridges identified on the Nigerian continental slope using 3-D seismic coherency. The Leading Edge, 18(5), 595-599.

NORMARK, W.R., PIPER, D.J.W. & HESS, G.R. (1979) Distributary channels, sand lobes, and mesotopography of Navy submarine fan, California Borderland, with applications to ancient fan sediments. Sedimentology, 26(6), 749-774.

PATACCI, M., HAUGHTON, P.D. & MCCAFFREY, W.D. (2014) Rheological complexity in sediment gravity flows forced to decelerate against a confining slope, Braux, SE France. Journal of Sedimentary Research, 84, 270-277.

PEAKALL, J., MCCAFFREY, B. & KNELLER, B. (2000) A process model for the evolution, morphology, and architecture of sinuous submarine channels: Journal of Sedimentary Research, 70, 434–448.

PICKERING, K.T. & CORREGIDOR, J. (2005) Mass-transport complexes (MTCs) and tectonic control on basin-floor submarine fans, middle Eocene, south Spanish Pyrenees. Journal of Sedimentary Research, 75(5), 761-783.

POPRAWSKI, Y., BASILE, C., AGIRREZABALA, L., JAILLARD, E., GAUDIN, M. & JACQUIN, T. (2014) Sedimentary and structural record of the Albian growth of the Bakio salt diapir (the Basque Country, northern Spain). Basin Research, 26(6), 746-766.

POPRAWSKI, Y., BASILE, C., JAILARD, E., GAUDIN, M., AND LOPEZ, M. (2016) Halokinetic sequences in carbonate systems: An example from the Middle Albian Bakio Breccias Formation (Basque Country, Spain). Sedimentary Geology, 334, 34-52.

POSTMA, G. (1984) Mass-flow conglomerates in a submarine canyon: Abrioja fan-delta, Pliocene, southeast Spain. In: Sedimentology of Gravels and Conglomerates, Canadian Society of Petroleum Geologists Memoir (Ed. by Koster, E.H. & Steel, R.J.), 10, 237-258.

POSTMA, G. (1984) Slumps and their deposits in fan delta front and slope (sedimentation model, Spain). Geology, 12(1), 27-30.

POSTMA, G., NEMEC, W. & KLEINSPEHN, K. (1988) Large floating clasts in turbidites: a mechanism for their emplacement. Sedimentary Geology, 58 (1), 47-61.

POSTMA, G., HILGEN, F.J. & ZACHARIASSE, W.J. (1993) Precession-punctuated growth of a late Miocene submarine-fan lobe on Gavdos (Greece). Terra nova, 5(5), 438-444.

PRÉLAT, A., HODGSON, D.M. & FLINT, S.S. (2009) Evolution, architecture and hierarchy of distributary deep-water deposits: a high-resolution outcrop investigation from the Permian Karoo Basin, South Africa. Sedimentology, 56(7), 2132-2154.

PRÉLAT, A. & HODGSON, D.M. (2013) The full range of turbidite bed thickness patterns in Submarine lobes: Controls and implications. Journal of the Geological Society, v. 170(1), pp. 209-214.

PUGA-BERNABÉU, Á., WEBSTER, J., BEAMAN, R., REIMER, P. & RENEMA, W. (2014)

Filling the gap: A 60ky record of mixed carbonate-siliciclastic turbidite deposition from the Great Barrier Reef. Marine and Petroleum Geology, 50, 40-50.

REMACHA, E. & FERNÁNDEZ, L.P. (2003) High-resolution correlation patterns in the turbidite systems of the Hecho Group (South-Central Pyrenees, Spain). Marine and Petroleum Geology, 20, 711–726.

ORTIZ-KARPF, A., HODGSON, D.M. & MCCAFFREY, W.D. (2015) The role of mass-transport complexes in controlling channel avulsion and the subsequent sediment dispersal patterns on an active margin: the Magdalena Fan, offshore Colombia. Marine and Petroleum Geology, 64, 58-75.

OSLEGER, D.A. & MONTAÑEZ, I.P. (1996) Cross-platform architecture of a sequence boundary in mixed siliciclastic-carbonate lithofacies, Middle Cambrian, southern Great Basin, USA. Sedimentology, 43(2), 197-217.

SAINTOT, A., STEPHENSON, R.A., STOVBA, S., BRUNET, M.F., YEGOROVA, T. & STAROSTENKO, V. (2006) The evolution of the southern margin of Eastern Europe (Eastern European and Scythian platforms) from the latest Precambrian-Early Palaeozoic to the Early Cretaceous: Geological Society, London, Memoirs, 32(1), 481-505.

SALLER, A.H., BARTON, J.W. & BARTON, R.E. (1989) Slope sedimentation associated with a vertically building shelf, Bone Spring Formation, Mescalero Escarpe field, southeastern New Mexico. In: Controls on carbonate platform and basin development (Ed. by P.D. Crevello, J.J. Wilson, J.F. Sarg, and J.F. Read), Society of Economic Paleontologists and Mineralogists, pp. 275-288.

SCOTT, E., GELIN, F., JOLLEY, S., LEENAARTS, E., SADLER, S. & ELSINGER, R. (2010) Sedimentological control of fluid flow in deep marine turbidite reservoirs: Pierce Field, UK Central North Sea. Geological Society Special Publication, 347, 113-132.

SOBIESIAK, M.S., KNELLER, B., ALSOP, G.I. & MILANA, J.P. (2016) Inclusion of substrate blocks within a mass transport deposit: a case study from Cerro Bola, Argentina. In: Submarine Mass Movements and Their Consequences, pp. 487-496. Springer.

SOHN, Y.K. (2000) Depositional processes of submarine debris flows in the Miocene fan deltas, Pohang Basin, SE Korea with special reference to flow transformation. Journal of Sedimentary Research, 70, 491–503.

SOHN, Y., CHOE, M. & JO, H. (2002) Transition from debris flow to hyperconcentrated flow in a submarine channel (the Cretaceous Cerro Toro formation, southern Chile). Terra Nova, 14(5), 405-415.

SOSSON, M., STEPHENSON, R., SHEREMET, Y., ROLLAND, Y., ADAMIA, S., MELKONIAN, R., KANGARLI, T., YEGOROVA, T., AVAGYAN, A., GALOYAN, G. & DANELIAN, T. (2016) The eastern Black Sea-Caucasus region during the Cretaceous: New evidence to constrain its tectonic evolution. Comptes Rendus Geoscience, 348(1), 23-32.

SOUTTER, E.L., KANE, I.A. & HUUSE, M. (2018) Giant submarine landslide triggered by Paleocene mantle plume activity in the North Atlantic. geology, 46(6), 511-514.

SOUTTER, E.L., KANE, I.A., FUHRMANN, A., CUMBERPATCH, Z.A. & HUUSE, M. (2019) The Stratigraphic Evolution of Onlap in Clastic Deep-marine Systems: Autogenic Modulation of Allogenic Signals. Journal of Sedimentary Research, 89 (10), 890-917.

SPYCHALA, Y.T., HODGSON, D.M., PRÉLAT, A., KANE, I.A., FLINT, S.S. & MOUNTNEY, N.P. (2017) Frontal and lateral submarine lobe fringes: comparing sedimentary facies, architecture and flow processes. Journal of Sedimentary Research, 87, 75-96.

STEVENSON, C.J., JACKSON, C.A-L., HODGSON, D.M., HUBBARD, S.M. & EGGENHEISEN, J.T. (2015) Deep-marine sediment bypass: Journal of Sedimentary Research, 85, 1058-1081.

STOW, D.A.V. & MAYALL, M. (2000) Deep-marine sedimentary systems: new models for the 21st
Century. Marine and Petroleum Geology, 17, 125-135

STRAUB, K., PAOLA, C., MOHRIG, D., WOLINSKY, M. & GEORGE, T. (2009) Compensational stacking of channelized sedimentary deposits. Journal of Sedimentary Research, 79, 673-688.

SURLYK, F. (1984) Fan-delta to submarine fan conglomerates of the Volgian-Valanginian Wollaston Forland Group, East Greenland. In: Sedimentology of Gravels and Conglomerates: Canadian Soc. of Petroleum Geologists, Memoir (Ed. by E. H. Koster & R. J. Steel), 10, 359-382.

SUMNER, E.J., PEAKALL, J., PARSONS, D.R., WYNN, R.B., DARBY, S.E., DORRELL, R.M., MCPHAIL, S.D., PERRETT, J., WEBB, A. & WHITE, D. (2013) First direct measurements of hydraulic jumps in an active submarine density current. Geophysical Research Letters, 40, 5904-5908.

SYLVESTER, Z. & LOWE, D.R. (2004) Textural trends in turbidites and slurry beds from the Oligocene flysch of the East Carpathians, Romania. Sedimentology, 51, 945–972.

TALLING, P., MASSON, D. SUMNER, E. & MALGESINI, G. (2012) Subaqueous sediment density flows: Depositional processes and deposit types. Sedimentology, 59, 1937-2003.

TASSY, A., CROUZY, E., GORINI, C., RUBINO, J.L., BOUROULLEC, J.L. & SAPIN, F. (2015) Egyptian Tethyan margin in the Mesozoic: Evolution of a mixed carbonate-siliciclastic shelf edge (from Western Desert to Sinai). Marine and Petroleum Geology, 68, 565-581.

TERLAKY, V., ROCHELEAU, J. & ARNOTT, R.W.C. (2016) Stratal composition and stratigraphic organization of stratal elements in an ancient deep-marine basin-floor succession, Neoproterozoic Windermere Supergroup, British Columbia, Canada. Sedimentology, 63(1), 136-175

TINTERRI, R., LAPORTA, M. & OGATA, K. (2017) Asymmetrical cross-current turbidite facies tract in a structurally-confined mini-basin (Priabonian–Rupelian, Ranzano Sandstone, northern Apennines, Italy). Sedimentary Geology, 352, 63–87.

TUCKER, M.E. (2003) Mixed clastic–carbonate cycles and sequences: Quaternary of Egypt and Carboniferous of England. Geologia Croatica, 56(1), 19-37.

VAN WAGONER J.C., MITCHUM R.M., CAMPION K.M. & RAHMANIAN V.D. (1990) Siliciclastic Sequence Stratigraphy in Well Logs, Cores, and Outcrop: Concepts for High-Resolution Correlation of Facies. American Association of Petroleum Geologists Methods in Exploration Series, pp. 55.

VINCENT, S.J., MORTON, A.C., CARTER, A., GIBBS, S. & BARABADZE, T.G. (2007) Oligocene uplift of the Western Greater Caucasus: an effect of initial Arabia–Eurasia collision. Terra Nova, 19(2), 160-166.

WAGREICH, M. & KRENMAYR, H. (2005) Upper Cretaceous oceanic red beds (CORB) in the Northern Calcareous Alps (Nierental Formation, Austria): Slope topography and clastic input as primary controlling factors. Cretaceous Research, 26(1), 57-64.

WALKER, R.G. (1978) Deep-marine sandstone facies and ancient submarine fans: Models for exploration for stratigraphic traps. AAPG Bulletin, 62, 932-966.

WALKER, W., JOBE, Z. R., WOOD, L. & SARG, R. (2019) Progradational Slope Architecture and Sediment Partitioning in the Outcropping Mixed Siliciclastic-Carbonate Bone Spring Formation, Permian Basin, west Texas. EarthArXiv

WANG, C., HU, X., SARTI, M., SCOTT, R. & LI, X. (2005) Upper Cretaceous oceanic red beds in southern Tibet: A major change from anoxic to oxic, deep-sea environments. Cretaceous Research, 26(1), 21-32.

WESCOTT, W.A. & ETHRIDGE, F.G. (1983). Eocene fan delta-submarine fan deposition in the Wagwater Trough, east-central Jamaica. Sedimentology, 30(2), 235-247.

YOSE, L.A. & HELLER, P.L. (1989) Sea-level control of mixed-carbonate-siliciclastic, gravity-flow deposition: Lower part of the Keeler Canyon Formation (Pennsylvanian), southeastern California. Geological Society of America Bulletin, 101(3), 427-439.

ZELLER, M., VERWER, K., EBERLI, G.P., MASSAFERRO, J.L., SCHWARZ, E. & SPALLETTI, L. (2015) Depositional controls on mixed carbonate–siliciclastic cycles and sequences on gently inclined shelf profiles. Sedimentology, 62(7), 2009-2037.

ZONNEVELD, J.P., MOSLOW, T.F. & HENDERSON, C.M. (1997) Lithofacies associations and depositional environments in a mixed siliciclastic-carbonate coastal depositional system, upper Liard Formation, Triassic, northeastern British Columbia. Bulletin of Canadian Petroleum Geology, 45(4), 553-575.

FIGURES

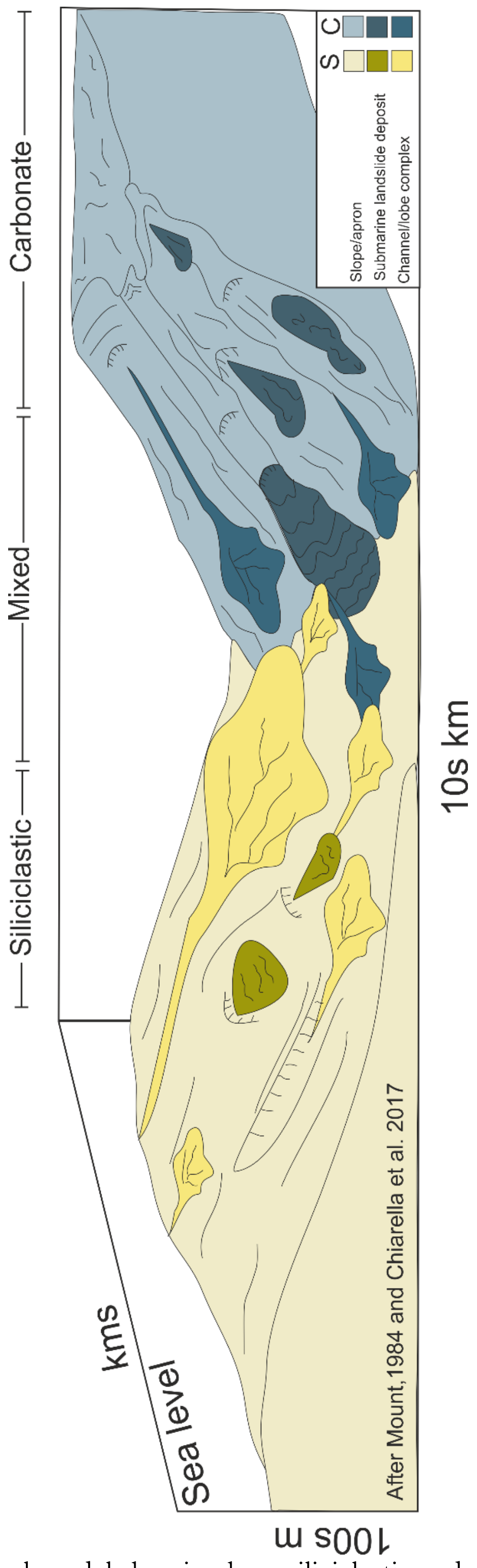

Figure 1: Simplified conceptual model showing how siliciclastic and carbonate systems may interact at a basin-scale in a deep-marine mixed siliciclastic-carbonate system. Carbonate material is shed from a shallower carbonate-producing platform that periodically received siliciclastic material; this is then redeposited in the deep-marine by of gravity flows (After Mount 1984, Chiarella et al. 2017).

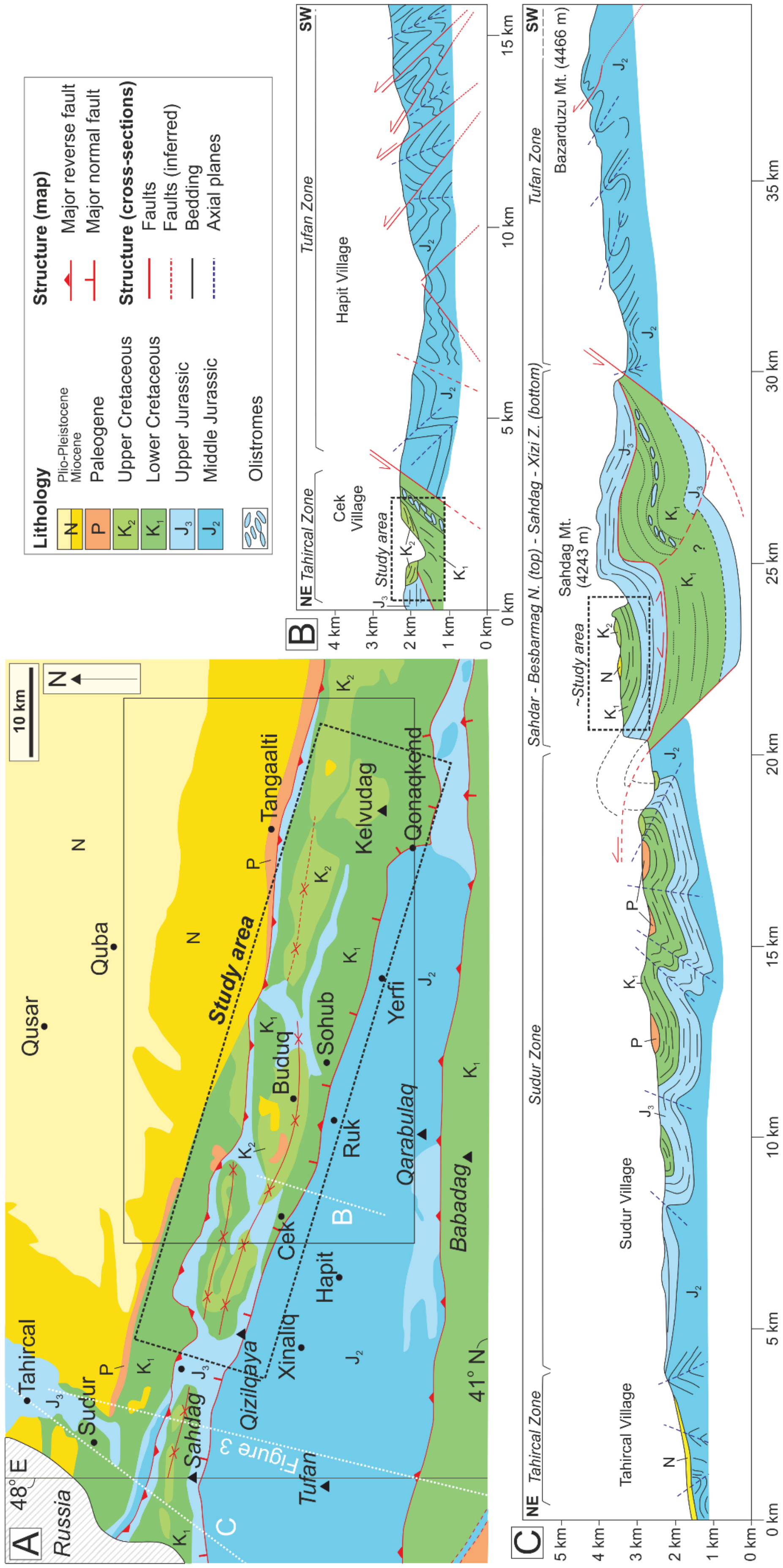

A
Russia
48° E
41° N
10 km
N
Tahircal
Sudur
Sahdag
Tufan
Qizilqaya
Xinaliq
Hapit
Cek
Buduq
Sohub
Ruk
Qarabulaq
Babadag
Yerfi
Kelvudag
Qonaqkend
Tangaalti
Quba
Qusar
Study area
Figure 3
B
C
Lithology
Plio-Pleistocene
Miocene
Paleogene
Upper Cretaceous
Lower Cretaceous
Upper Jurassic
Middle Jurassic
Olistromes
Structure (map)
Major reverse fault
Major normal fault
Structure (cross-sections)
Faults
Faults (inferred)
Bedding
Axial planes
NE
SW
Tahircal Zone
Tufan Zone
Cek Village
Hapit Village
Study area
Sudur Zone
Tahircal Village
Sudur Village
Sahdag Mt. (4243 m)
~Study area
Bazarduzu Mt. (4466 m)
Sahdar - Besbarmag N. (top) - Sahdag - Xizi Z. (bottom)
0 km
5 km
10 km
15 km
20 km
25 km
30 km
35 km
1 km
2 km
3 km
4 km

Figure 2: Structural and stratigraphic framework of the Eastern Greater Caucasus (EGC) of Azerbaijan. A) Simplified geological map, black box locates study area, lines B and C are located. Schematic location of Figure 3 is shown. B) Cross section across the Cek-Hapit Valley, black box locates study area. C) Cross section from Tahircal-Sahdag Mountain – Bazarduzu Mountain, black box locates equivalent stratigraphy to our studied section (Modified from Bochud, 2011).

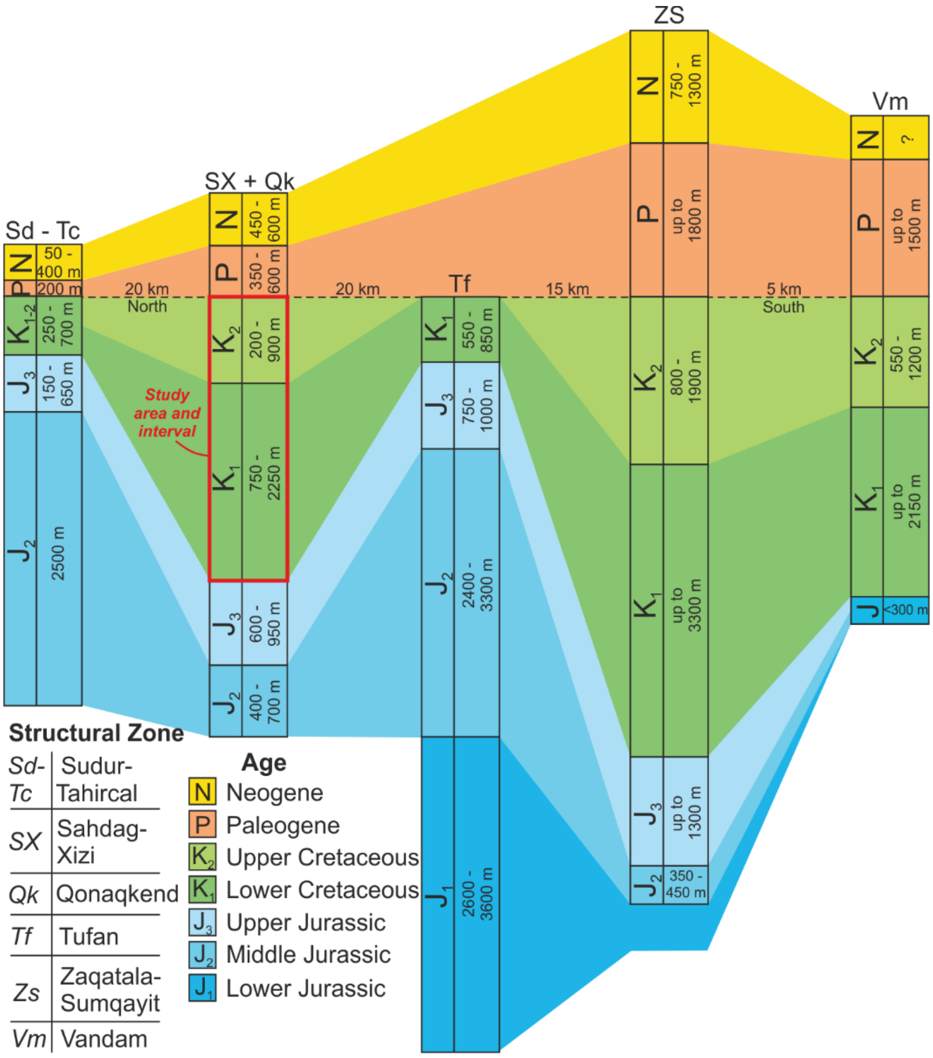

Figure 3: Stratigraphic section trending roughly north-south across the five main structural zones (from Bochud 2011) of the EGC. Flattened along the top of the Cretaceous, located on Figure 2.

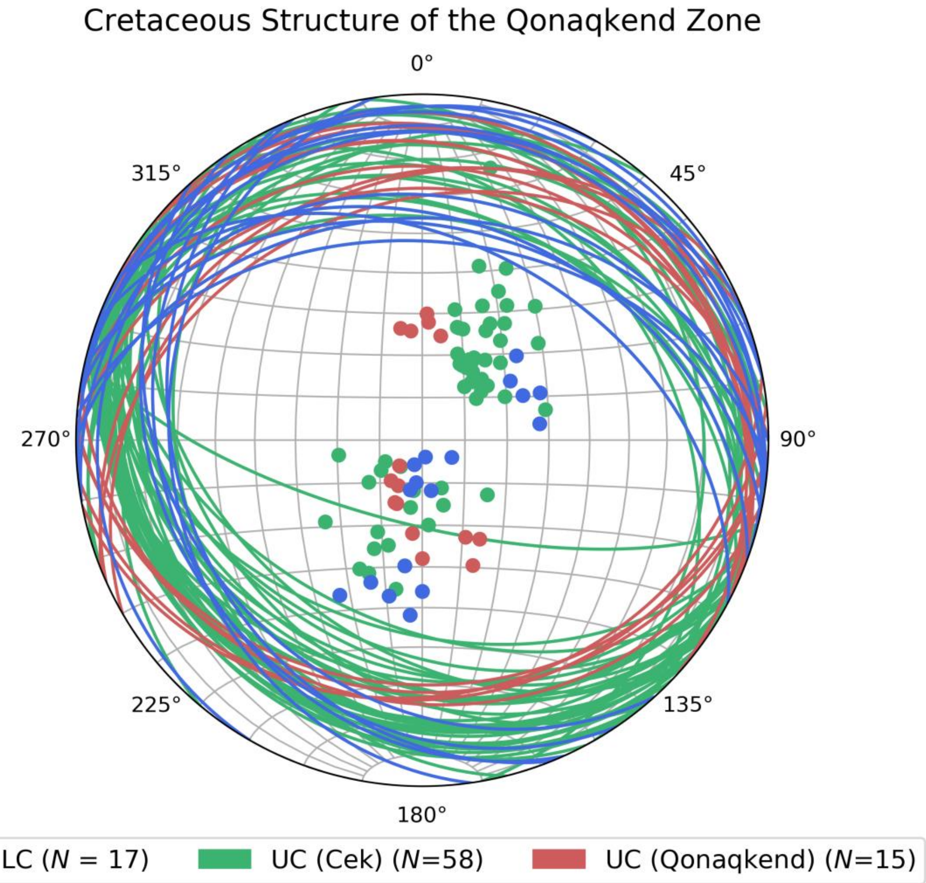

Figure 4: Equal area stereographic projection showing bedding readings for Cretaceous stratigraphy across Qonaqkend Zone. Bedding planes shown as lines and poles to bedding shown as dots. Coloured by stratigraphy and location; LC- Lower Cretaceous, UC- Upper Cretaceous. Structural data reveals a shallow-moderate structural dip to the north and south, in agreement with the east-west trending structural zones of the EGC.

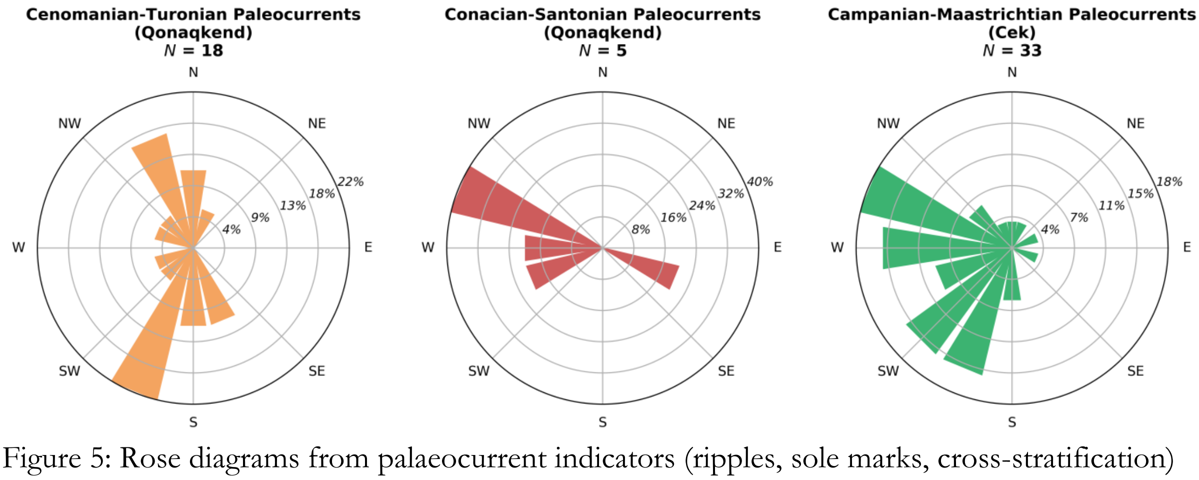

Figure 5: Rose diagrams from palaeocurrent indicators (ripples, sole marks, cross-stratification) from the Cretaceous stratigraphy of the Qonaqkend Zone. Readings have been corrected for tectonic tilt and are subdivided by stratigraphy and location (see Figure 2).

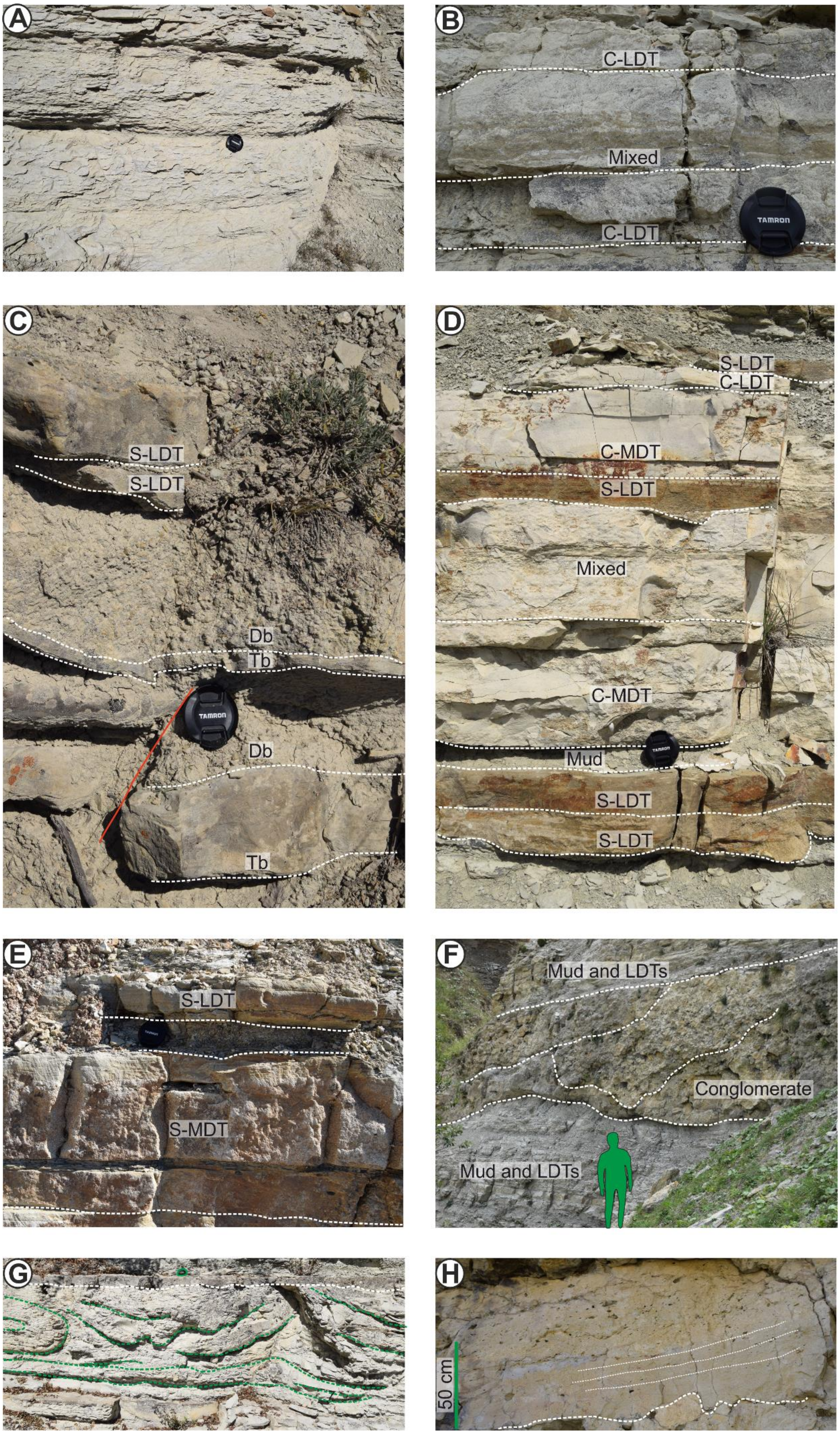
A
B
C-LDT
Mixed
C-LDT
C
S-LDT
S-LDT
Db
Tb
Db
Tb
D
S-LDT
C-LDT
C-MDT
S-LDT
Mixed
C-MDT
Mud
S-LDT
S-LDT
E
S-LDT
S-MDT
F
Mud and LDTs
Conglomerate
Mud and LDTs
G
H
50 cm

Figure 6: Facies photographs. Facies described in detail in Table 1. Scale is either lens cap (52 mm), person (1.74 m) or indicated. LDT; low density turbidite, MDT; medium density turbidite, Db; debrite (poorly sorted clast rich deposit); Tb; Turbidite, S; Siliciclastic, C; Calcareous. A) Calcareous mudstone B) Calcareous low density turbidite and mixed beds (of siliciclastic and calcareous low density turbidites). C) Two bi-partite beds consisting of a lower turbidite and an upper debrite, in this case both siliciclastic, overlain by two siliciclastic low density turbidites. D) Evidence for facies scale mixing (sensu Chiarella et al. 2017); calcareous turbidites were recognised in the field by their pale cream colour, while siliciclastic turbidites were brown-orange in colour and contained visual quartz granules. Calcareous turbidite probably accumulated slowly based on their grain size, and were punctuated by siliciclastic gravity flows, forming mixed beds. E) Siliciclastic low and medium density turbidites with cm-scale mud clasts weathered out. F) Mudstone and low density turbidites (both calcareous and siliciclastic) punctuated by metre-scale amalgamated conglomerates. G) Chaotic, clast rich-deposit with deformed, non-extensive bedding. Camera lens cap circled in green. H) Erosionally-based, crudely cross-laminated siliciclastic high density turbidite rich in mud clasts.

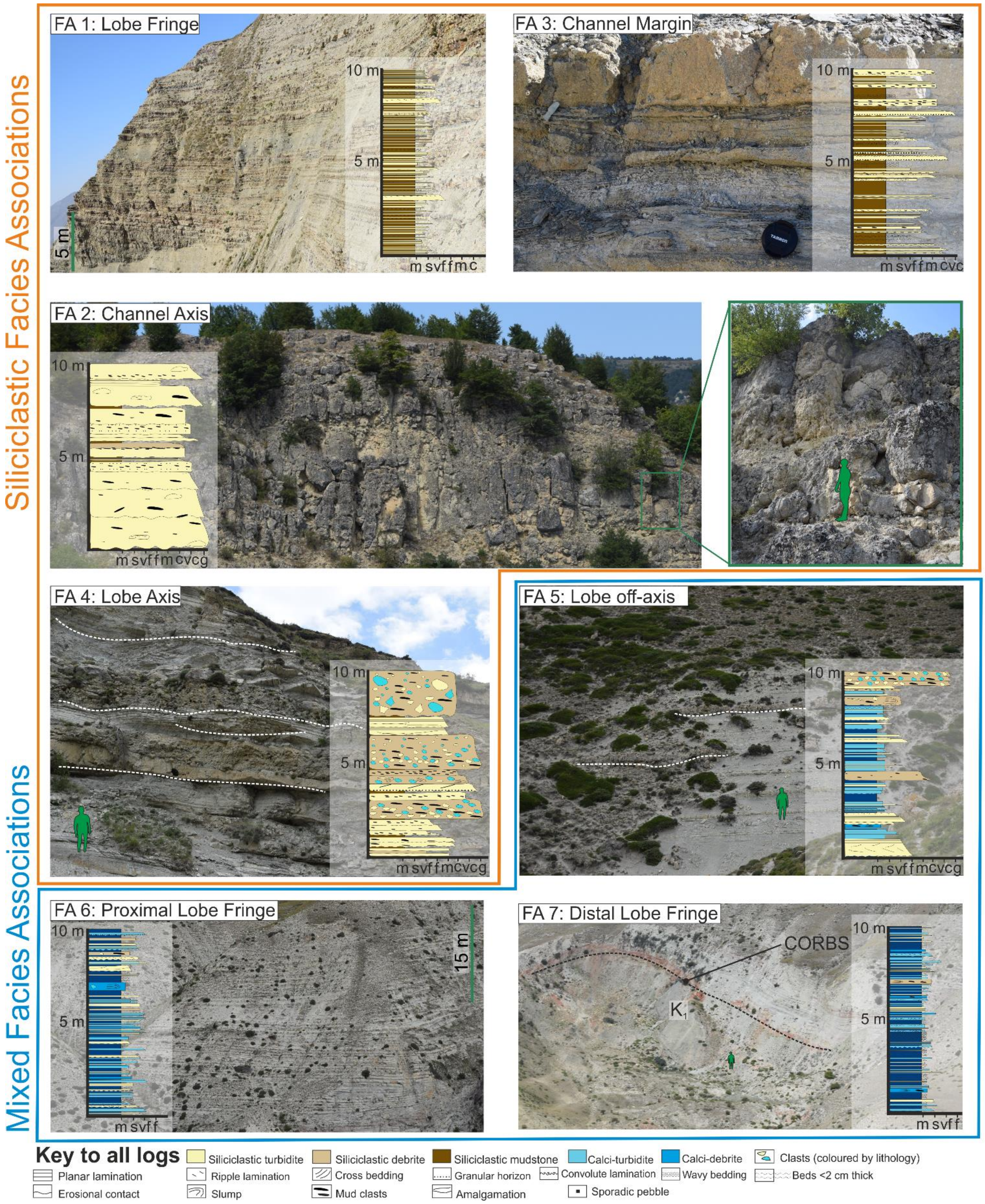

Figure 7: Type examples of the seven recognised facies associations, divided into siliciclastic and mixed (siliciclastic and calcareous) associations, by orange and blue boxes respectively. Scale either lens cap (52 mm), person (1.74 m) or indicated. 10 m type log is taken from representative logged section of each facies association. Cretaceous Oceanic Red Beds; CORBS.

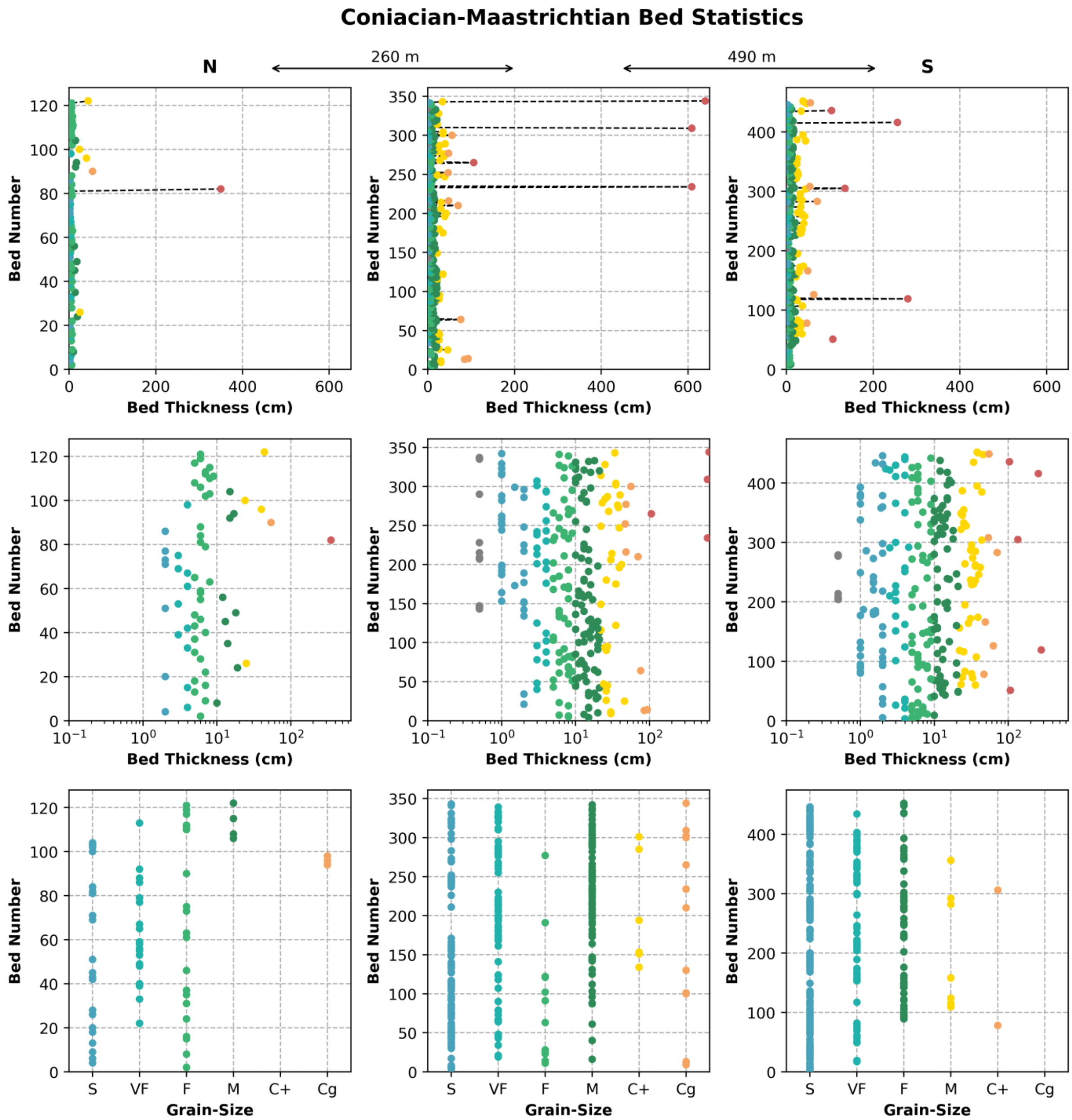

Figure 8: Quantative facies analysis for Coniacian-Maastrichtian stratigraphy. The three columns represent three different logged sections from north to south that are representative of northern margin, axis and southern margin of the basin respectively. Charts compare bed number (with 1 being at the base of the log and 200 at the top) to bed thickness (linearly in the top column and logarithmically in the middle column) and logged grain size (in the basal column). Where grain size varies within the bed average grain size is used. In the top column thick beds are highlighted with a dashed line. Colours are for visual separation of data, and meaning changes per column, blue are thin/fine beds/grain-size, oranges are thick/coarse beds/grain-sizes. Scales for bed number vary across the rows.

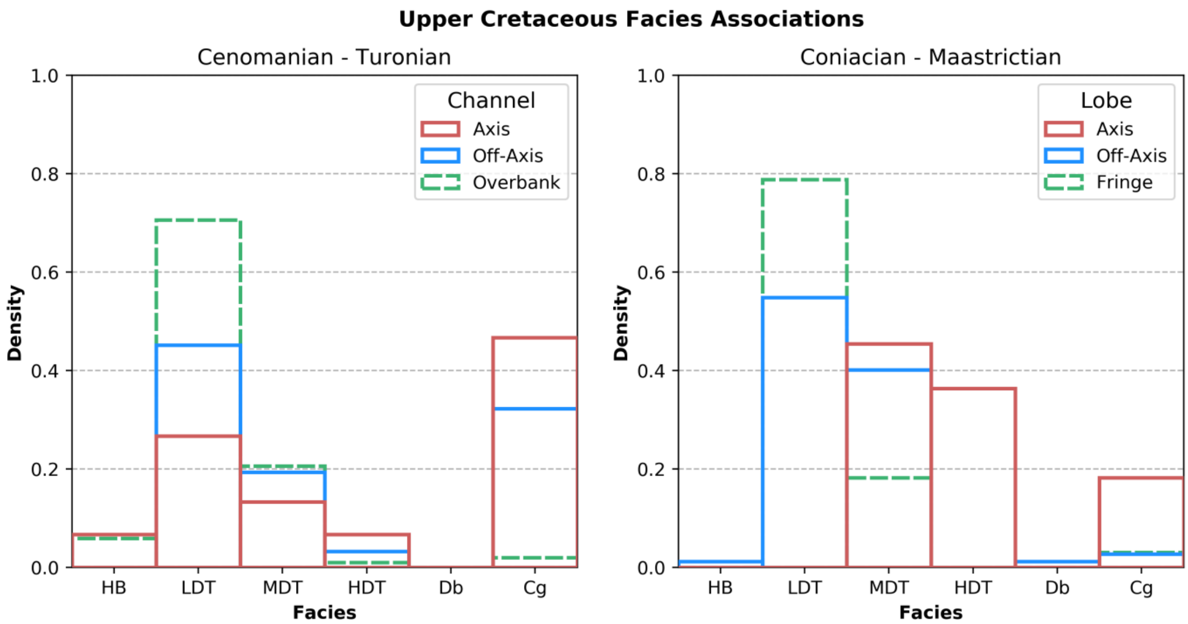

Figure 9: Quantative facies analysis for Upper Cretaceous stratigraphy, divided into Cenomanian-Turonian channelised siliciclastic deposition and Coniacian – Maastrictian mixed lobe deposition. Facies refer to HB: hybrid bed (bi and tri-partite beds); LDT: low density turbidite; MDT: medium density turbidite; HDT: high density turbidite; Db: debrite (poorly sorted clast rich deposit) and Cg: conglomerate. Coloured by type log for different sub-environment. Density refers to the percentage of each facies in each log.

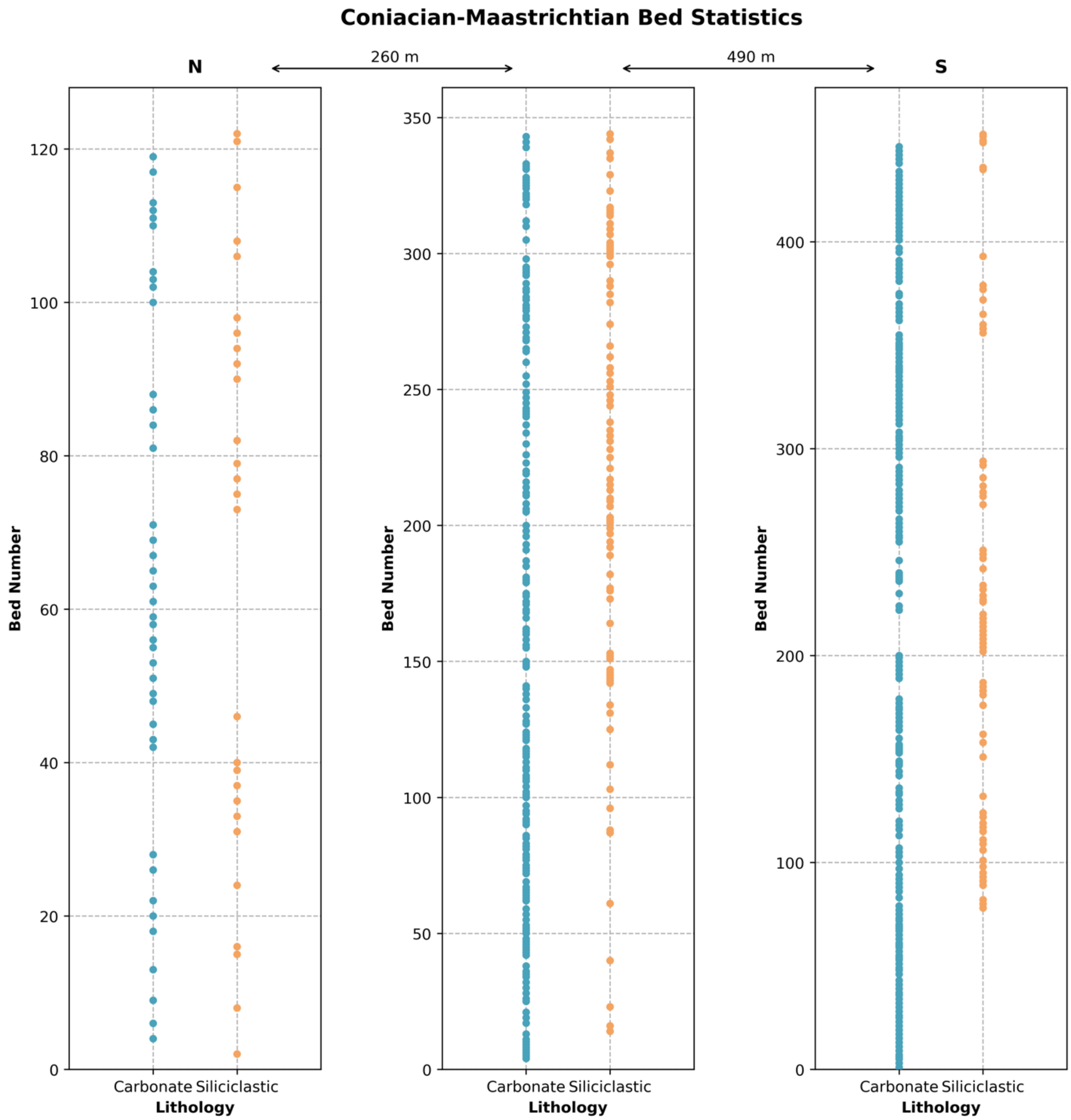

Figure 10: Quantative facies analysis of Coniacian-Maastrichtian mixed stratigraphy comparing bed composition (carbonate or siliciclastic) against bed number (height up log). Using the same logged sections as Figure 8, and thus a different number of beds per log resulting in variable bed number scale.

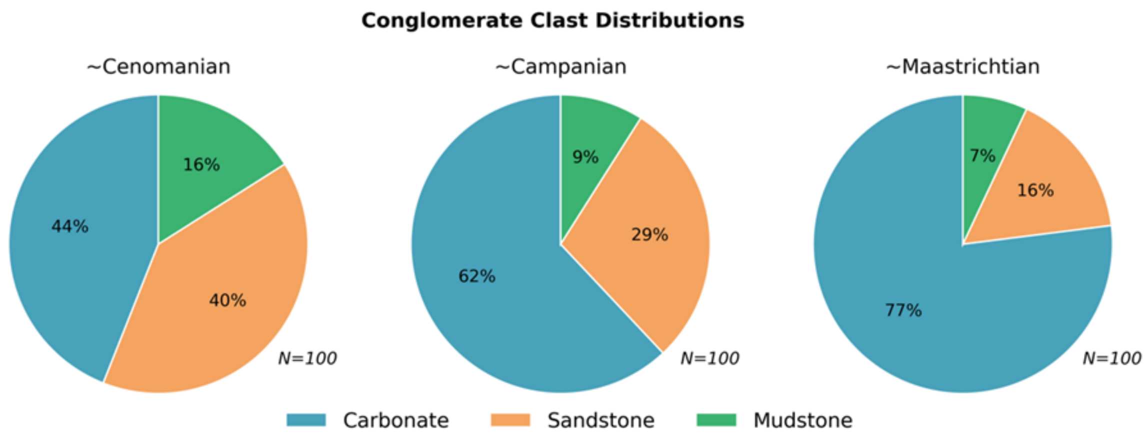

Figure 11: Pie charts showing composition of clasts within conglomerates per stratigraphic age, taken from 100 clasts from representative conglomeratic beds of over 1 metre thick. Percentage equates to absolute number of clasts, as 100 are sampled. Carbonate clast content increases through time, discussed in text.

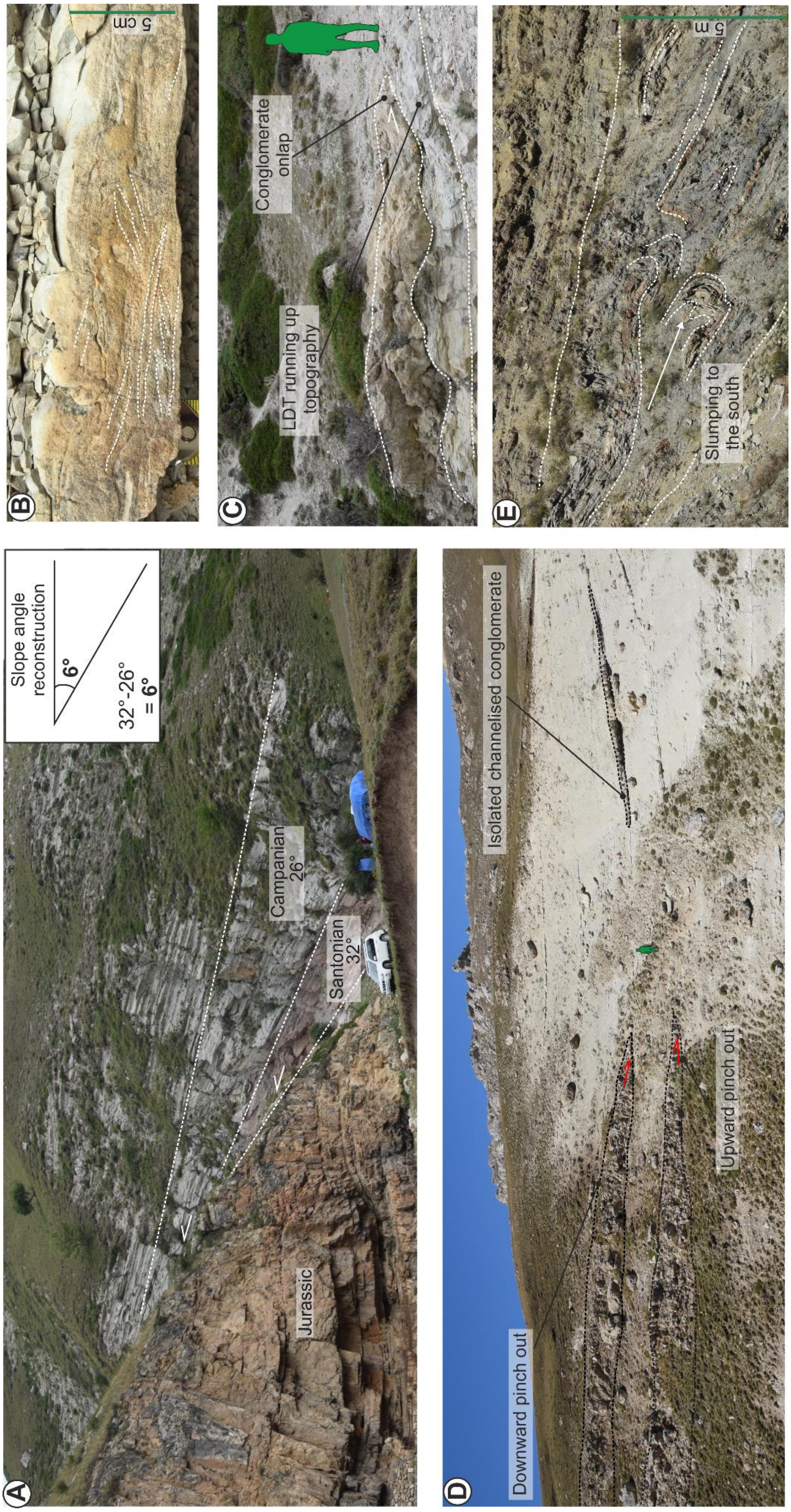

A
Slope angle reconstruction
6°
32°-26° = 6°
Campanian 26°
Santonian 32°
Jurassic
B
5 cm
C
Conglomerate onlap
LDT running up topography
D
Isolated channelised conglomerate
Downward pinch out
Upward pinch out
E
5 m
Slumping to the south

Figure 12: Evidence for palaeotopography. Scale indicated by person (1.74m), car (1.9 m) or indicated. A) Cretaceous stratigraphy thinning and onlapping Jurassic limestone, slope angle reconstructed. B) Evidence for opposing ripple directions suggesting flow reflection. C) Thickness and pinch-out variability of different deposits on a metre-scale laterally. D) Cliff section containing three conglomerate bodies which vary in architecture and termination style as indicated. E) Submarine landslide deposit showing evidence for slumping towards the south.

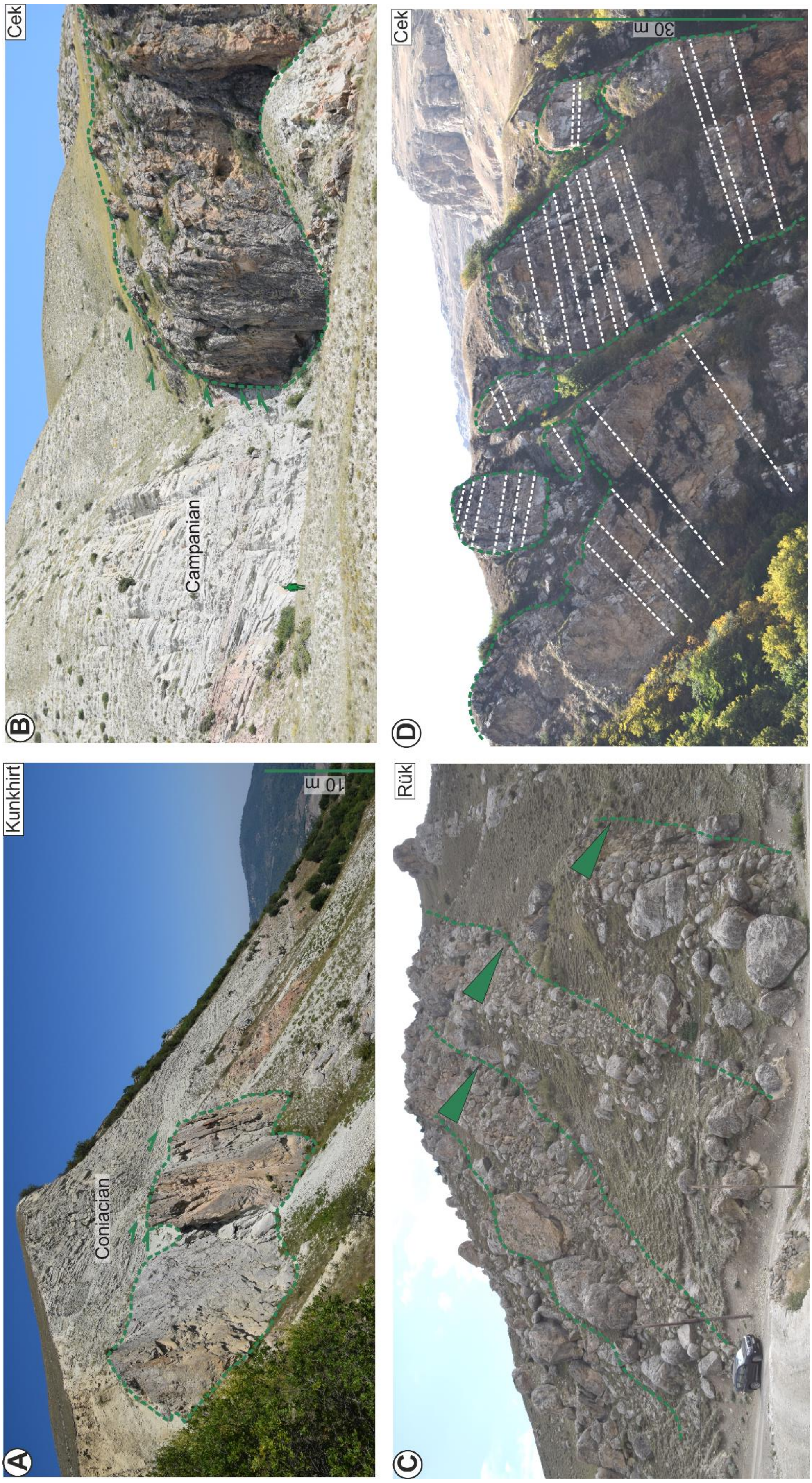
A
Kunkhirt
Coniacian
10 m
B
Cek
Campanian
C
Rük
D
Cek
30 m

Figure 13: Evidence for collapse of the Jurassic carbonate platform. Scale is shown by person (1.74 m), car (1.9 m) or indicated. Onlap indicated by green arrows, extent of clast or bedding surface shown in green dashed line. A) Metre-scale limestone clasts within Coniacian mixed stratigraphy at Kunkhirt. B) Campanian calcareous low density turbidites abutting against a decametre-scale Jurassic limestone block at Cek. C) Stacked, inversely-graded submarine landslide deposits primarily composed of reworked Jurassic limestone blocks at Rük, upwards widening triangles indicate coarsening upwards (inverse-grading). D) In situ break-up of the Jurassic platform at Cek. Clasts are fractured and separated but bedding planes (indicated in white) are still visible showing minimal displacement.

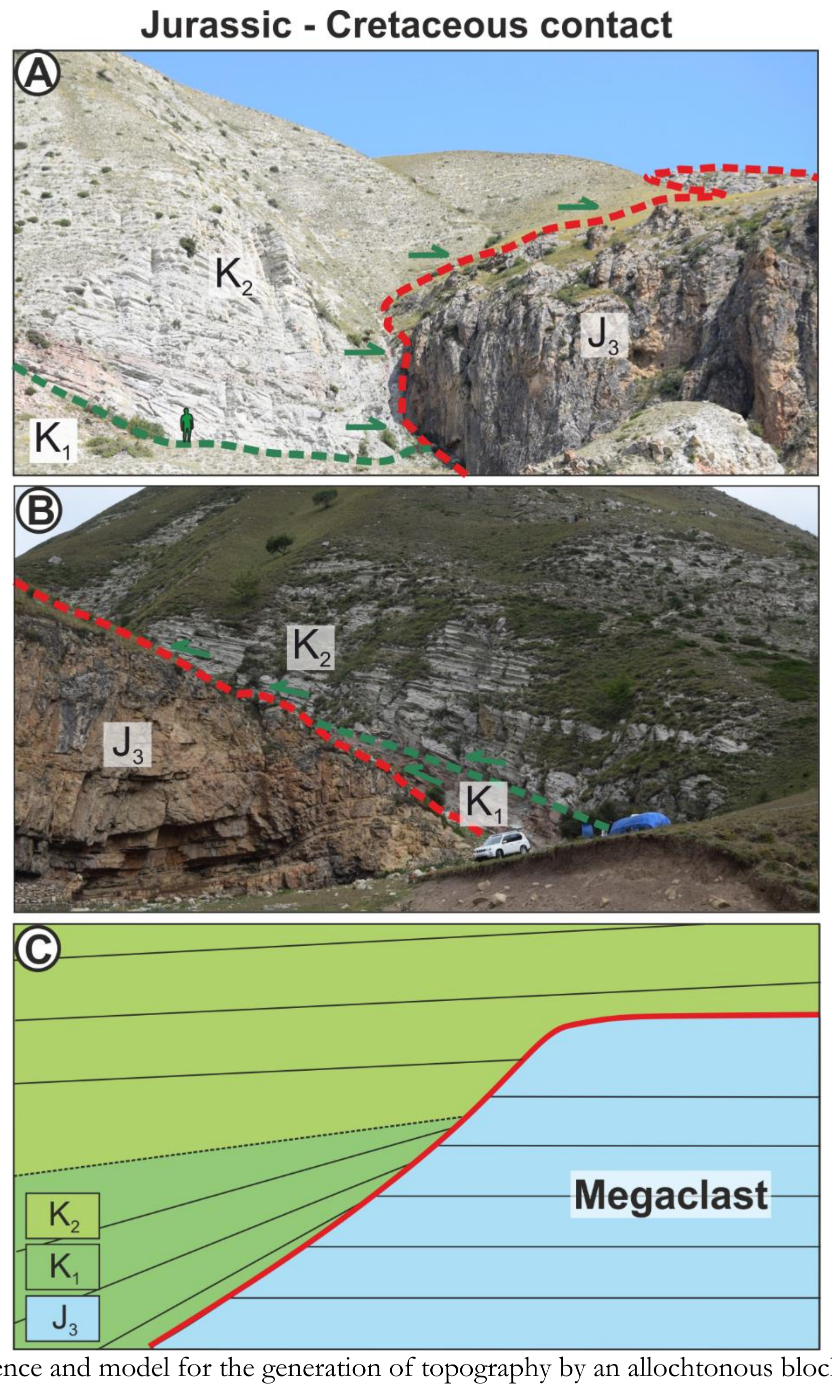

Figure 14: Evidence and model for the generation of topography by an allochtonous block throughout the Cretaceous. A&B) field examples of Jurassic stratigraphy forming topography throughout the Cretaceous influencing sediment routing. C) Schematic model showing formation of topography.

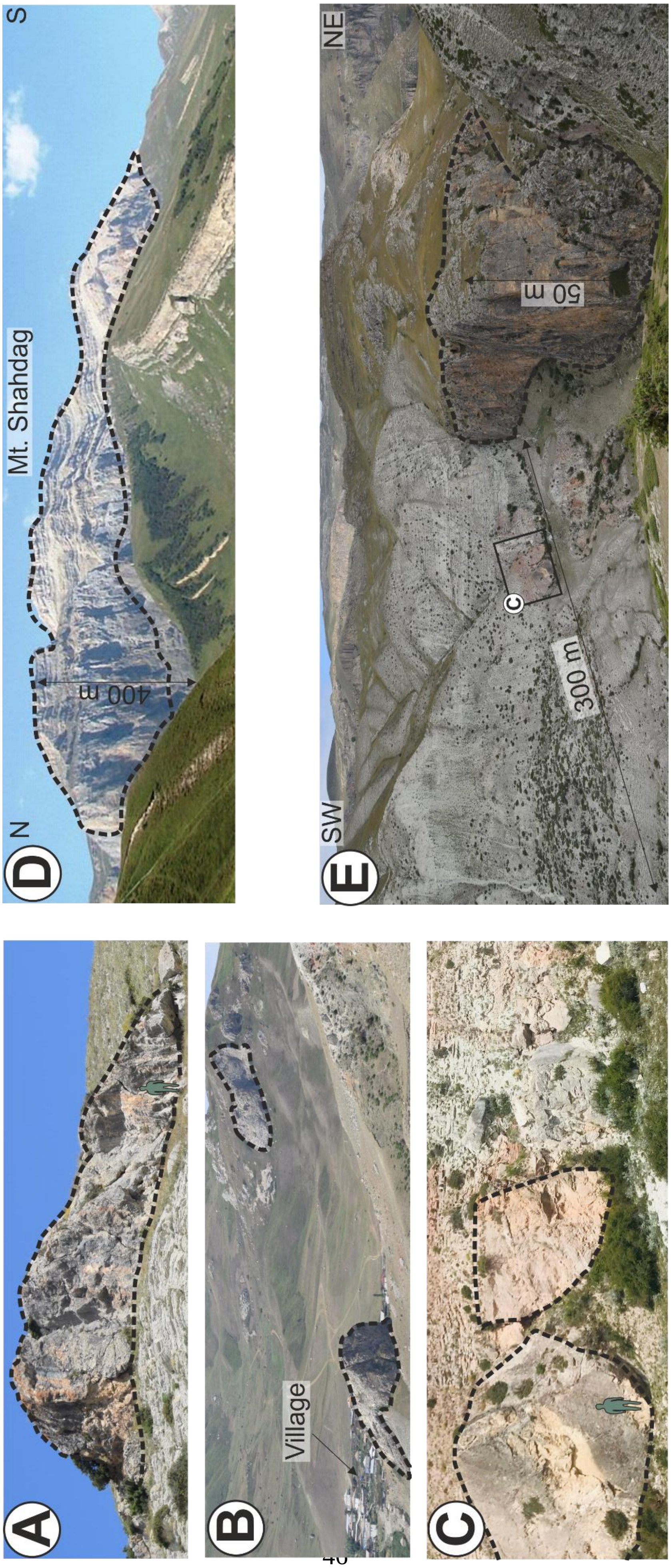
A
B
Village
C
D
N
S
Mt. Shahdag
400 m
E
SW
NE
300 m
50 m
c

Figure 15: Evidence for allochtonous block model as the most likely for the generation of Cretaceous topography. Scale is shown by person (1.74 m) or indicated. Blocks are drawn around with black dashed line. A-C are examples of metre-decametre scale clasts around Cek. D) Shahdag Mountain, the tallest mountain in Azerbaijan, is interpreted as a kilometre-scale wide olistostrome by Bochud, 2011. E) Block with both margins exposed and onlapped by mixed stratigraphy, black box locates C.

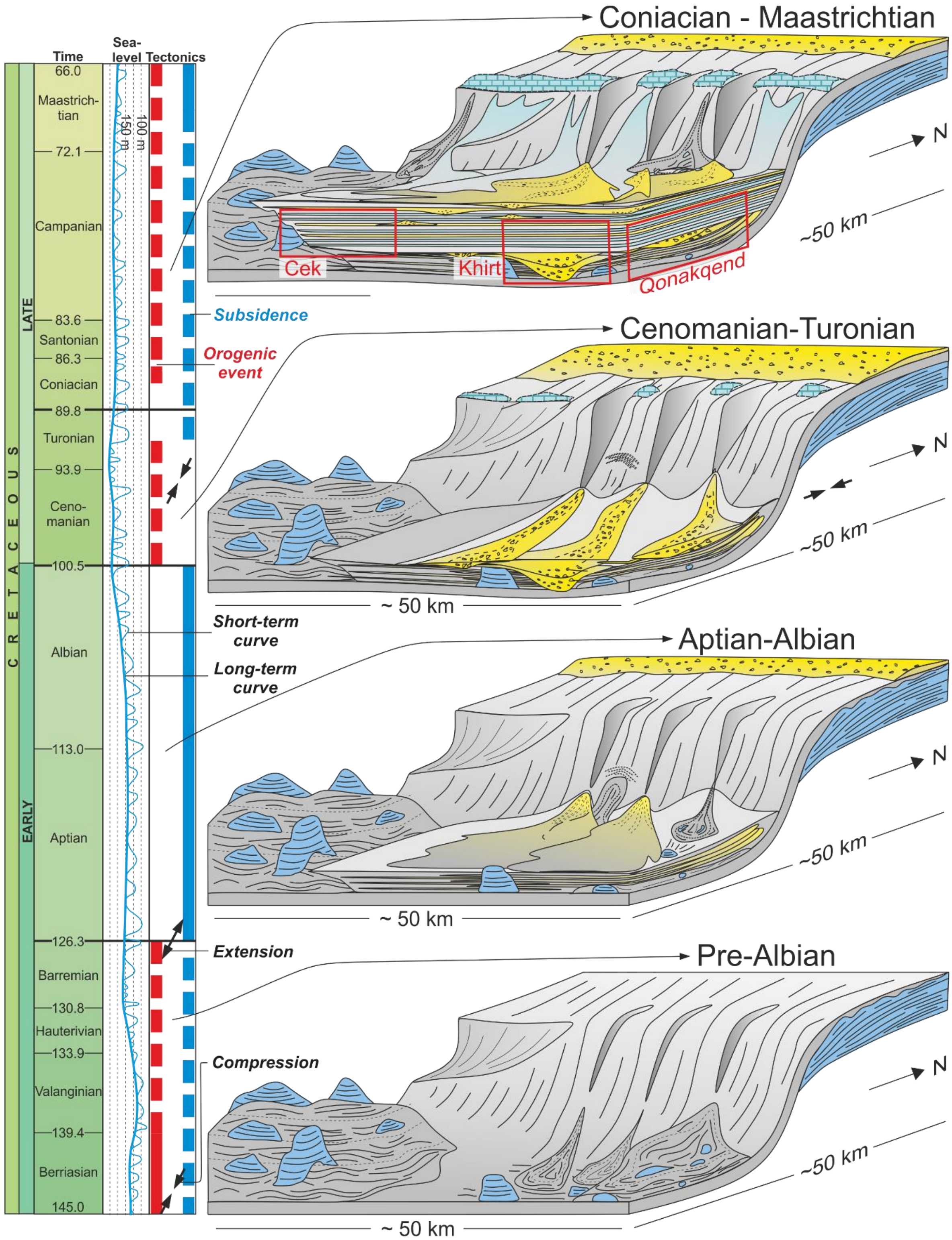

Figure 16: Evolutionary model for the Cretaceous of the study area. Studied stratigraphic sections highlighted. Topography, thought to be formed by a mega-clast, is present throughout the Cretaceous and influences deposition, discussed in text. Extract from the geological time column, sea level fluctuations and local tectonic events highlighted on the left. The Pre-Albian was dominated by limestone blocks on a muddy slope. Thin-bedded siliciclastics of a distal lobe were deposited during the Aptian-Albian. Siliciclastic channels are prominent throughout the Cenomanian-Turonian. In the Coniacian-Maastrichtian mixed calcareous and siliciclastic lobes, of different sub-environments interact, and are likely sourced from the same northern margin.

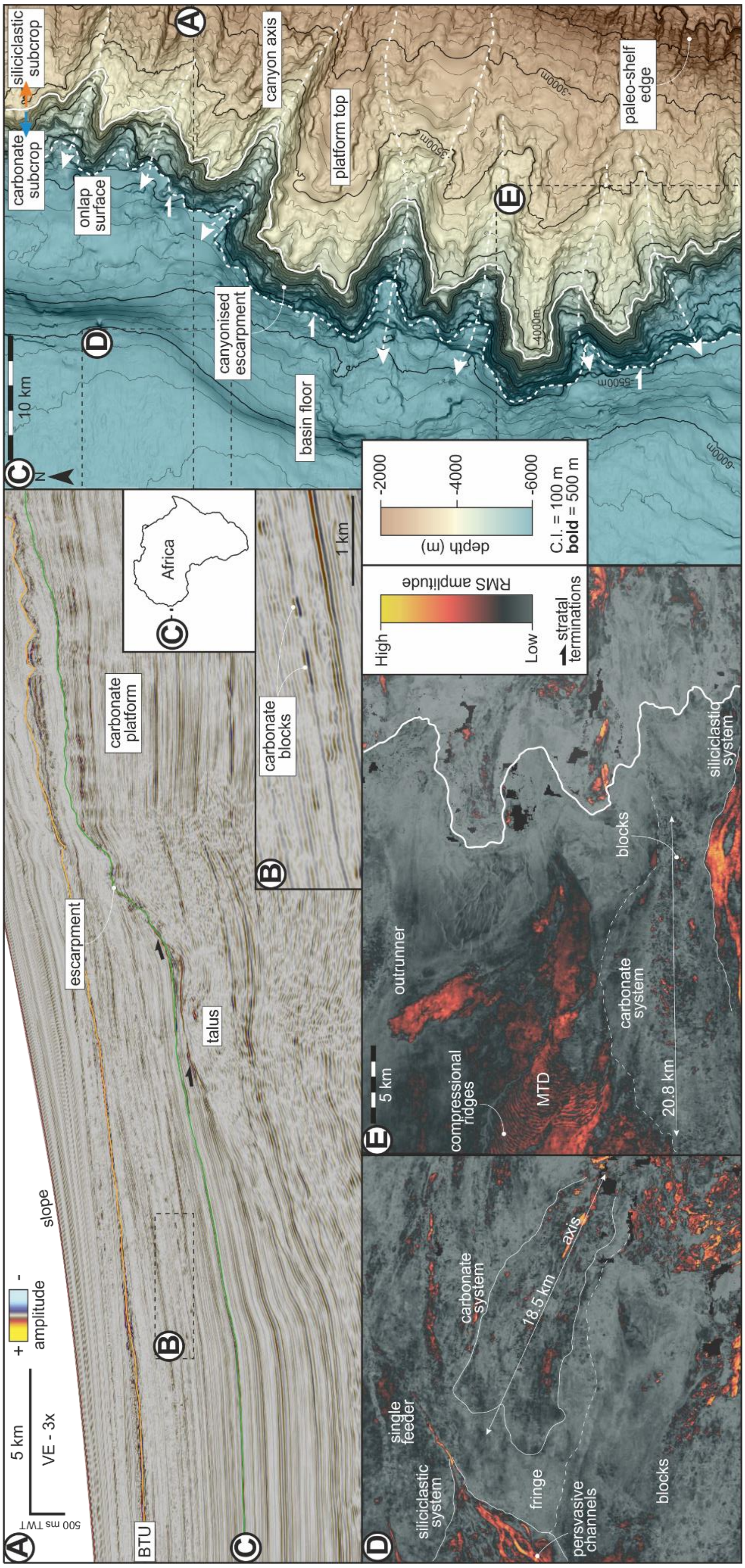
A
500 ms TWT
5 km
VE - 3x
amplitude
slope
BTU
escarpment
talus
carbonate platform
B
carbonate blocks
1 km
Africa
C
siliciclastic subcrop
carbonate subcrop
onlap surface
canyon axis
platform top
paleo-shelf edge
canyonised escarpment
basin floor
10 km
N
-3000m
-3500m
-4000m
-5500m
-6000m
depth (m)
-2000
-4000
-6000
C.I. = 100 m
bold = 500 m
RMS amplitude
High
Low
stratal terminations
D
siliciclastic system
single feeder
fringe
pervasive channels
carbonate system
18.5 km
axis
blocks
E
5 km
compressional ridges
MTD
outrunner
carbonate system
20.8 km
blocks
siliciclastic system

Figure 17: Seismic geomorphology of a mixed-system offshore The Gambia, NW Africa. A) East-West two-way time seismic section with key stratigraphic surfaces, location shown in C. B) Enlarged two-way time seismic section of carbonate blocks observed in the deep-marine mixed-system. C) Depth structure map (contoured) with dip magnitude below of the diachronous regional composite unconformity surface displayed on seismic section A, showing the heavily canyonised carbonate escarpment margin, canyon flow pathways (dashed white lines), lithological contact between siliciclastic and carbonate subcrop (solid white line) and onlap surface (dotted white line). D & E) RMS amplitude maps extracted from a +/- 12 ms window around two Late Cretaceous horizons in the basin. Location of maps shown on C.

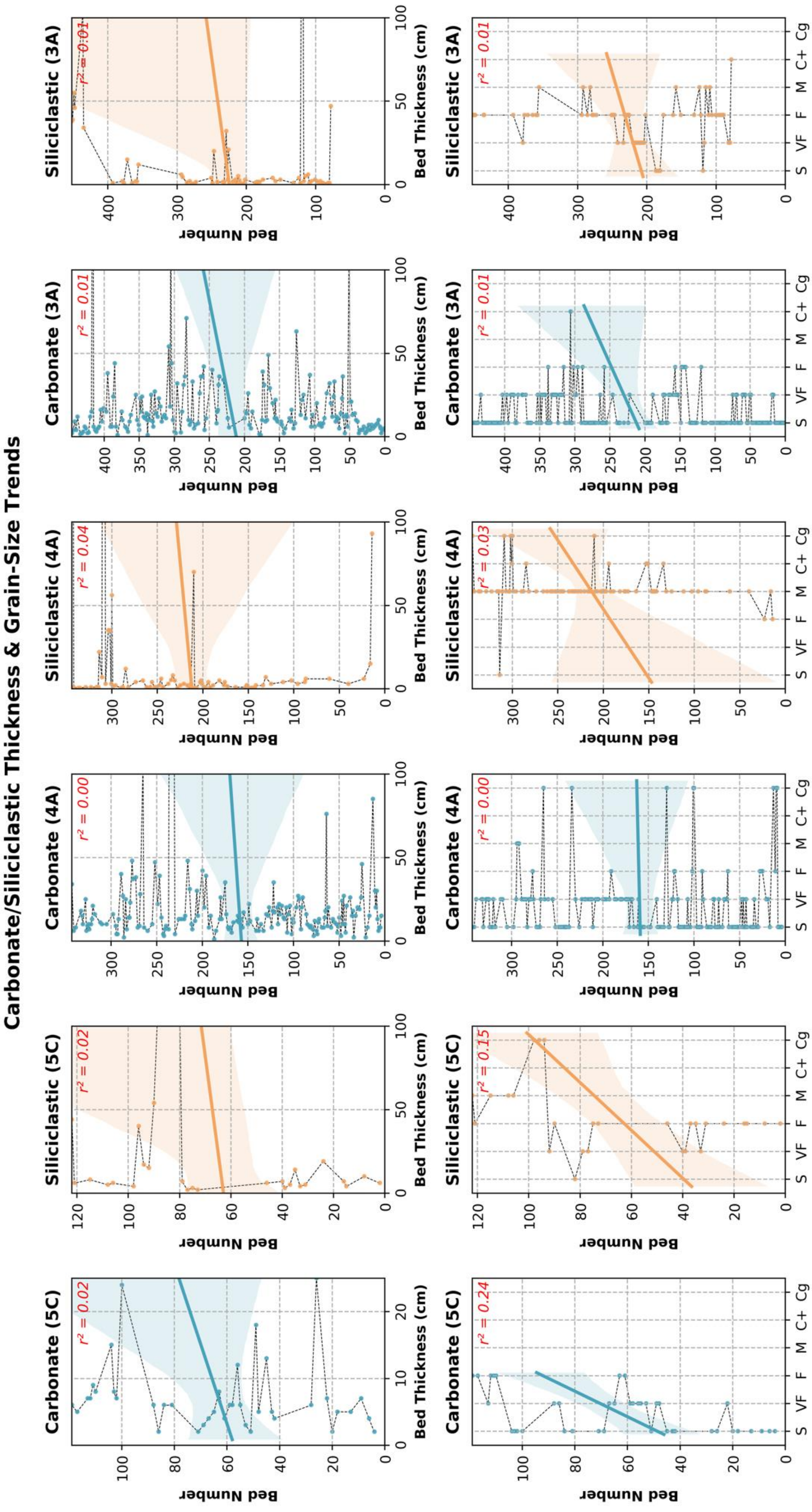

Carbonate/Siliciclastic Thickness & Grain-Size Trends
Siliciclastic (3A)
r² = 0.01
Carbonate (3A)
r² = 0.01
Siliciclastic (4A)
r² = 0.04
r² = 0.03
Carbonate (4A)
r² = 0.00
r² = 0.00
Siliciclastic (5C)
r² = 0.02
r² = 0.15
Carbonate (5C)
r² = 0.02
r² = 0.24
Bed Number
Bed Thickness (cm)
Grain-Size
S VF F M C+ Cg

Figure 18: Quantitative facies analysis for Coniacian-Maastrichtian stratigraphy. Logs are the same as Figures 8 and 10. 5C, 4A and 3A represent northern margin, axis and southern margin respectively. Each log is divided into carbonate and siliciclastic beds, and bed number is plotted against bed thickness (upper row) and grain size (bottom row). Lines indicate linear regression, r^2 value is labelled in red, shading either side of the line indicates a 95% confidence interval for the linear regression (trend line). Low-no correlation is observed suggesting no stacking patterns or modulation of any stacking patterns by interaction of both systems, discussed in text.

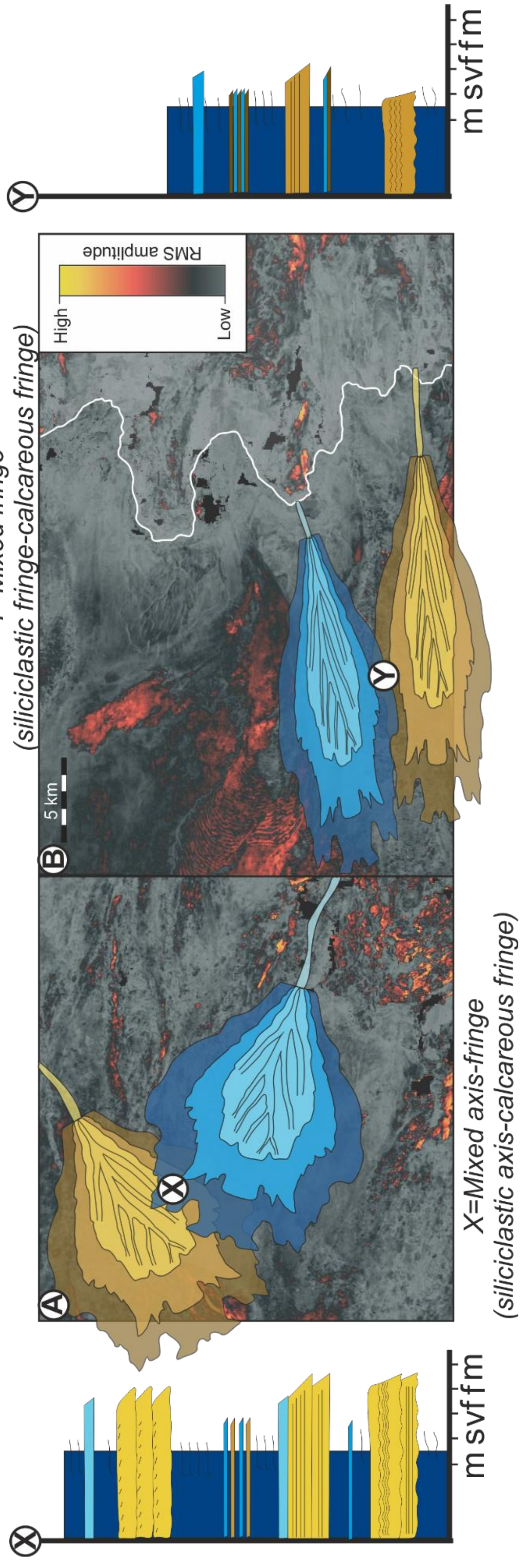

Figure 19: Schematic showing potential interactions of calcareous and siliciclastic lobes in mixed systems. A and B are RMS maps from Figure 17, which have been overlain by lobe complex

geometries, as an interpretation based on seismic facies analysis and understanding of regional source area (see Casson et al. 2020). X and Y represent log/core through locations where the lobe complexes interact in A and B respectively. X crosses the lobe fringe of the calcareous system and the lobe axis of the siliciclastic system and Y crosses the lobe fringe of both systems resulting in a thinner and finer grained succession when compared to X. This variability highlights difficulties arising from exporting sub-environment terminology developed in siliciclastic systems (e.g. Prélat et al. 2009) into mixed systems